



Arab American University
Faculty of Graduate Studies

**Thickness and Post Annealing Effects on the Structural,
Optical and Dielectric Properties of Copper Oxide Thin
Films**

By

Alaa Ayman Ekmal

Supervisor

Prof. Dr. Atef Fayez Qasrawi

This thesis was submitted in partial fulfillment of the
requirements for The Master's degree in

Physics

September/2018

Thickness and Post Annealing Effects on the Structural, Optical and Dielectric Properties of Copper Oxide Thin Films

By

Alaa Ayman Ekmail

This thesis was defended successfully on 30/9/2018 and approved by:

Committee members

Signature

1. Prof. Dr. Atef Fayez Qassrawi (supervisor)

.....

2. Assoc. Prof. Dr. Ahmad Omar

.....

3. Dr. Iyad Saadeddin

.....

Declaration

The work provided in this thesis, unless otherwise referenced, is the researcher's own work and has not been submitted elsewhere for any other degree or qualification.

Student's Name:

Signature:

Date:

Dedectioon

To My Parents

To My husband

Acknowledgments

All Thanks go to my god who gives me the ability to finish this thesis and peace be on our prophet Mohammad.

I am grateful to my parents and my husband, who have provided me with moral and emotional support in my life. I am also grateful to my other family members and friends who supported me .

A very special gratitude goes to Prof. Atef Qasrawi due his effort with me to produce a valuable scientific thesis, and for supporting me throughout my university life.

With a special mention to Dr. Muayed Abu Saa, who supervise my bachelors thesis, that put me on the beginning of the master.

I am also grateful to my teachers, Dr. Adli Saleh, Prof. Dr. Zaki Saleh, and Prof. Mohammed Abu Samra.

Special thanks to my university Arab American University, and all supervisors and administration in AAUP.

Thickness and Post Annealing Effects on the Structural, Optical and Dielectric Properties of Copper Oxide Thin Films

Abstract

In this work, the thin film thickness and the post annealing effects on the structural, compositional and optical properties of copper oxide thin films are explored by means of X-ray diffraction, energy dispersive X-ray spectroscopy and ultraviolet-visible-near infrared light spectrophotometry techniques, respectively. Particularly, various thin films of copper oxide, which exhibit thicknesses in the range of 50-1000 nm were produced by the physical vapor deposition technique (thermal type) under vacuum pressure of 10^{-5} mbar. The films thicknesses effect on the crystalline nature and the optical transmittance, reflectance, absorbance as well as energy band gap. The dielectric spectra are determined to identify the most appropriate thickness for optoelectronic applications. It is observed that while films of thicknesses of 50 – 100 nm exhibit indirect allowed electronic transition band gap, films of larger thicknesses exhibit direct allowed transition energy band gap. In addition, the analysis of the absorption coefficient spectra in the low absorption region have shown that the 1000 nm thin film has band tail. The deposited 1000 nm thin film was also annealed in vacuum at 250 °C temperature. The effect of annealing temperature on structural, optical and dielectric properties was studied using different characterization techniques. The XRD analysis confirmed the enhanced crystallinity of the 1000 nm thick sample. The optical band gaps of the annealed 1000 nm CuO thin film was measured to be 3.30 and 2.30 eV, and it exhibit no band tail after annealing. On the other hand, a dielectric

constant spectrum which is carried out in the energy range of 1.1-4.0 eV exhibit decreasing values with increasing sample thickness. The imaginary part of the dielectric spectra is modeled in accordance with the hole-plasmon interaction to reveal the optical conductivity parameters. The evaluated parameters have shown that the CuO thin films can be employed as optical resonators with relatively acceptable optical conductivity suitable for visible light communications.

List of contents

	Chapter Title	Page No.
Chapter one	Introduction And Literature Survey	1
	1.1 Introduction And Literature Review	1
	1.2 Applications	5
	1.3 Problem Statement	5
Chapter Two	Theoretical Background	7
	2.1 Crystalline nature	7
	2.2 The X-ray Diffraction	7
	2.3 Optical properties of metal oxide	9
	2.3.1 Absorption of light in matter	10
	2.3.2 Energy band gab	11
	2.3.3 Energy band tail	16
	2.3.4 Dielectric spectra	17
Chapter Three	Experimental Details	23
	3.1 Sample Preparation	23
	3.2 X-ray Diffraction Technique	25
	3.3 Optical Measurements	27
	3.5 Hot probe technique	28
Chapter four	Result and Discussion	30
	4.1 Structural properties	30
	4.2 Energy dispersive X-ray analysis	31
	4.3 Optical properties	33
	4.4 Dielectric dispersion	44
	4.5 Annealing process	52
	4.5.1 Structural properties	52

	4.5.2 Optical properties	54
	4.5.3 Dielectric properties	58
Chapter Five	Conclusion	61

List of tables

Table No.	Table Title	Page No.
4.1	The band gaps and band tails of the CuO thin films.	43
4.2	The computed parameters of the Plasmon-electron interactions in the CuO thin films	51
4.3	XRD analysis of annealed samples at 250°C	53
4.4	The band gaps and band tails of the 1000 nm CuO thin film after annealing.	57
4.5	The computed parameters of the Plasmon-electron interactions in the CuO thin films	60

List of figures

Fig. No	Fig. caption	Page No.
2.1	Deriving Bragg's Law using the reflection geometry and applying trigonometry.	8
2.2	Light reflectance ,transmittance and absorbance	10
2.3	Energy band gap of Insulator, Semiconductor and Metal	11
2.4	Energy band gap diagram.	12
2.5	Semiconductor band tail structure	16
3.1	a)Thermal evaporation system b)Annealing system	24
3.2	sample of copper oxide thin film (500 nm)	25
3.3	Schematic of x-ray diffraction	26
3.4	The X-ray diffraction technique	27
3.5	The UV-VIS spectrophotometer	28
3.6	Hot-probe set up	29
3.7	Hot-probe result	29
4.1	XRD patterns of Copper Oxide films measured at room temperature.	30
4.2	a): SEM image for as grown 1000 nm copper oxide film. b) and c) The x – ray diffraction patterns for the as grown 1000 nm copper oxide film	32
4.3	Transmission spectra of the CuO thin films measured at 300 K in the wavelength range of 300 to 1100 nm.	34
4.4	Reflection spectra of the CuO thin films measured at 300K in the wavelength range of 300 to 1100 nm at normal incidence.	35
4.5	Absorbance spectra of the CuO thin films measured at 300K in the energy range of 1.1 to 4.1 eV .	36
4.6	Absorption coefficient of Cupper Oxide thin films.	37

4.7	a) Energy band gaps investigation for the 50nm CuO thin films	39
	b) Energy band gaps investigation for the 100nm CuO thin films	40
	c) Energy band gaps investigation for the 250nm CuO thin films	40
	d) Energy band gaps investigation for the 500nm CuO thin films	41
	e) Energy band gaps investigation for the 1000nm CuO thin films	41
4.8	$\ln(\alpha) - E$ variation in the low absorption region for band tail investigation of the CuO thin films.	42
4.9	Real parts of the dielectric constant of the films measured in the frequency range of 300-1000 THz.	46
4.10	(a) Imaginary parts of the dielectric constant of the 50 nm CuO film measured in the frequency range of 300-1000 THz. (b) for 100 nm and 250 nm, and (c) for 500 nm and 1000 nm.	48
4.11	XRD patterns of Copper Oxide films annealed at 250 C° by using evaporation system	53
4.12	Transmission spectra of the CuO thin films annealed at 250°C in the wavelength range of 300 to 1100 nm.	54
4.13	Reflection spectra of the CuO thin films annealed at 250°C	55
4.14	Absorbance spectra of the CuO thin films annealed at 250°C	56
4.15	Energy band gaps investigation for the 1000 nm CuO thin films	56
4.16	$\ln(\alpha) - E$ variation in the low absorption region for band tail investigation of the annealed 1000 nm CuO thin films at 250°C	57
4.17	Real parts of the dielectric constant of the 1000 nm film measured in the frequency range of 300-1100 THz at 250°C annealed.	58
4.18	Imaginary part of the dielectric constant of the 1000 nm CuO film measured in the frequency range of 300-1000 THz at 250°C annealed	59

Chapter One

Introduction and Literature Survey

1.1 Introduction and literature survey

CuO thin films are semiconductors which attracted attention due to its potential applications in optoelectronics. They are also used as gas sensors and transparent conducting devices [1]. CuO thin films have the potential to be employed as solar cells [2]. Copper oxide films have advantages such as non-toxicity, low cost, abundantly available and comparatively simple to form oxide layers [3, 4].

The structure of CuO is monoclinic. In this structure the tetra molecular cells have lattice parameters of values of $a=4.692 \text{ \AA}$, $b=3.4283 \text{ \AA}$, $c=5.1370 \text{ \AA}$ and $\beta=99.546$ [5,6]. To improve the physical and electrical properties of CuO various doping agents were used. As for example, Ni-doped and undoped CuO films were prepared onto glass substrates using spin-coating technique [7]. Various doping concentrations (2, 4, 6, and 10 %) on these films were used. The polycrystalline nature of growth revealed a discriminatory increase along the (-311) (111), and (002) plane orientation directions. In addition the atomic force microscopy studies revealed that the surface morphologies of the films were not regular. The conglomerations of particles on the surface were also defined by scanning electron microscopy images. On the other hand, the electrical properties of CuO were explored by using a Hall Effect technique. It is reported that the hole mobility increased and free charge carrier concentration decreased with increasing Ni concentration. In addition, the increase in the band gap value from 2.03 to 2.22 eV upon doping CuO with 10 % Ni was observed [7].

CuO thin films were prepared by different methods some of which are listed below:

(1) Spray technique [8]: using spray pyrolysis technique to deposit CuO thin films onto glass substrates for molar concentrations of 0.1, 0.2 and 0.3. The formation of polycrystalline CuO thin films are reported to be monoclinic structure with grain sizes in the range of 35 - 54 nm .It shows improved crystalline nature of deposited films with increasing molar concentration. It was also reported that a decrease in micro strain and dislocation density can be achieved with increasing molar concentration (M). The microstructure of the thin film intended at 0.1 M displayed needle like grain growth while 0.2 M and 0.3 M CuO films had a pored structure. The EDAX spectrum was used to define the distribution of copper and oxygen in the samples. The richness of copper in the prepared samples was associated with increasing molar concentration.

(2) Radio frequency (R.F.) [9]: magnetron sputtering process using copper oxide target under argon (Ar) pressure, have been used to produce the anatase phase copper oxide thin films. It is seen that crystallization increases slightly with the increased thickness of film. The slow growth of crystallite sizes was supported by atomic force microscopy (AFM) images for the as-grown films and increasing thickness. By increasing thickness, the resistivity of CuO films was increased. The optical properties of prepared thin films were studied about the absorption and transmission spectra. The energy band gap was found to be in the range of (2.25 eV - 2.60 eV) as the film thickness increased from 20 nm to 200 nm.

(3) Cold spray technique (CS) [10]: This method is totally different from other coating processes because of the use of low temperatures where low temperature aids in retaining the original powder chemistry and phases in the coating, with changes only due to

deformation and cold-working. CS process produced a deposition free of oxides and other inclusions to any metal surface, and due to compressive stresses, the dense uniform deposit of any thickness with wrought-like microstructure are obtained [11].

(4) Chemical solution deposition (CSD) method with layer variation [12]: is a wet-chemical process that has been used to design a wide variety of amorphous and crystalline oxide thin films. CSD technique is recently gaining momentum for the fabrication of electrolyte materials for solid oxide fuel cells (SOFCs) due to its cost-effectiveness, high yield, and simplicity of the process requirements. With regular operation at quiet liquid surface, film formation is also very uniform [13].

(5) Sol-gel technique [14]: Sol-gel method is one of the well-established synthetic approaches to prepare novel metal oxide (NPs) as well as mixed oxide composites. This method has potential control over the textural and surface properties of the materials. Sol-gel method mainly undergoes in few steps to deliver the final metal oxide protocols and those are hydrolysis, condensation, and drying process. Sol-gel methods have often been used in combination with physical deposition techniques, the formation of the hybrid oxide, occurring during the annealing step [14]. Sol-gel methods of synthesis of nonmaterial's (materials of which a single unit is sized between 1 to 1000 nanometers) present many advantages, the preparation of hybrid oxides taking advantage from the ease of doping [15].

(6) Molecular beam-epitaxy method (MBE) [16]: Molecular beam epitaxy takes place in high vacuum or ultra-high vacuum (10^{-8} – 10^{-12} Torr). The most important aspect of MBE is the deposition rate (typically less than 3,000 nm per hour) that allows the films to grow epitaxially. These deposition rates require proportionally better vacuum to achieve the same impurity levels as other deposition techniques. The absence of carrier gases as well as

the ultra high vacuum environment results in the highest achievable purity of the grown films.

(7) Chemical vapor deposition (CVD) [8]: is a parent to a family of processes whereby a solid material is deposited from a vapor by a chemical reaction occurring on or in the vicinity of a normally heated substrate surface. The resulting solid material is in the form of a thin film, powder, or single crystal.

(8) Thermal oxidation [8]: Thermal oxidation of copper used to control the formation of photovoltaic active cupric oxide (CuO) phase against the cuprous oxide (Cu₂O) phase. The thermal oxidation of copper is governed by the outward lattice diffusion and grain boundary diffusion of copper ions at the interface. The lattice diffusion favors the formation of Cu₂O phase whereas grain boundary diffusion favors the formation of CuO phase. This method controls the phase formation of copper oxide to obtain more photoactive material that is CuO [17].

(9) Electrodeposition [8]: is a well-known conventional surface modification method to improve the surface characteristics, decorative and functional, of a wide variety of materials. Electrodeposition is one of the cheapest processes to deposit copper oxide thin films. Copper oxide was electrodeposited on the copper substrate and gold plated glass substrate in an electrolyte bath containing 0.2 M CuSO₄·5H₂O, 3 M lactic acid and NaOH. A Potentiostat/Galvanostat with silver chloride electrode (Ag/AgCl) as a reference electrode was used for electrodeposition. From visual inspection it was found that copper oxide film was black and adherent on copper substrate. In gold coated glass substrate copper oxide film was also black but bonding between the substrate and copper oxide film was not good. The SEM study reveal that the films become more compact and grain sizes

of copper oxide films decreases at more negative potentials in deposition potential range. EDS analysis shows that percentage of oxygen in the copper oxide films increases with more negative potentials at the deposition potential range. It was found that with increase of time more adherent and uniform film thickness occurs [18].

(10) Thermal evaporation deposition method : Others studied Structural, and optoelectronic properties of thin films fabricated by thermal evaporation ,and as such thermal evaporation was quickly ruled out as samples prepared by this method have lower values of carrier concentration n and mobility μ [19].

1.2 Applications

CuO has been used in solar cell research. At the University of Shiga, CuO layers were spin-coated at 100 nm thick on fluorine doped tin oxide (FTO) substrate. It was concluded that the formation of higher quality CuO thin films may improve future CuO cell efficiency [20]. Semiconductor oxides are a promising alternative to silicon-based solar cells because they possess high optical absorption and are composed of low cost materials [21]. Also, CuO has been used as a hole transfer layer and barrier layer for dye-sensitized solar cells [22], active layer in various types of solar cells [23], passive layer in solar-selective surfaces. It would make a good selective absorbing layer because of its high solar absorbance and low thermal emittance.

1.3 Problem statement

Copper oxide is a promising material which can be employed for photovoltaic issues owing to its energy band gap. However, the crystalline nature and large transparency of these

films make the absorbability of this material to visible light relatively low. To overcome this trouble various techniques were employed. However, none of these techniques was able to provide sufficient information about the absorbability of this material. For this reason, here in this work, we aim to engineering the optical properties of this material, through thickness and annealing control. The optimal thickness of these films will be determined. In addition some of the prepared samples will be annealed in vacuum media. The two methods, thickness, and annealing in vacuum will provide the information about the best method to prepare the films and use them in optoelectronics. CuO films are deposited onto ultrasonically cleaned glass substrates at room temperature using the thermal vapor deposition technique. Then the film thicknesses are controlled by thickness monitor in steps .Each cycle is proposed to different thickness. The thickness is valid in the range from 100-1000 nm. Some of the samples are subjected to X-ray diffraction measurements. All samples are subjected to optical transmittance and reflectance measurements at normal incidence. Thereafter, samples of highest optimized thickness are annealed in vacuum at 250 °C temperature.

Chapter Two

Theoretical Background

2.1 Crystalline nature

Crystal structure is the manner in which ions, atoms, or molecules are spatially arranged. It is a unique arrangement of atoms in a crystal. It is one of the most important parts of materials science and engineering as many properties of materials depend on their crystal structures. The amorphous structure is random arrangement of atoms. The importance of semiconductors arises from the serious realization of the properties of amorphous semiconductors which require not only knowing with one special field of science or engineering, but a detailed knowledge of results from the collective fields of chemistry, physics, metallurgy, and electrical engineering. Although the amorphous semiconductors compared with that of crystalline materials, and much fundamental experimental and theoretical work remains to be done, still much developed thought has been set up to the subject over the past 10 years and great steps have been made in understanding the basic principles [24, 25].

2.2 The X-ray diffraction

The X-ray diffraction (XRD) technique is used to explore the crystallography. The interference pattern of X-rays scattered by crystals can be inferred from the geometry shown in Fig. 2.1

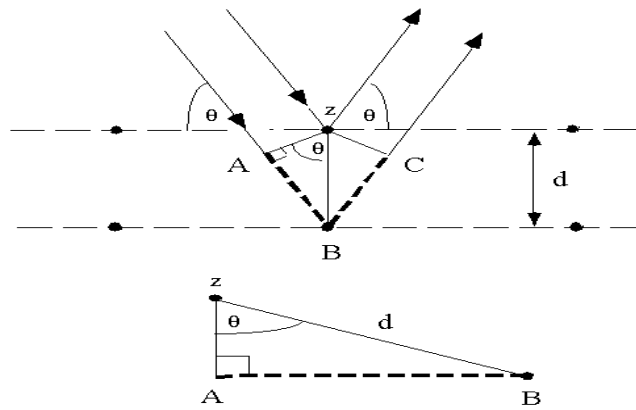


Figure 2.1: Deriving Bragg's Law using the reflection geometry and applying trigonometry.

The constructive interference occurs only when:

$$n\lambda = AB + BC \quad (2.1)$$

But as: $AB=BC$, So:

$$n\lambda = 2AB \quad (2.2)$$

$$\sin \theta = AB/d \quad (2.3)$$

$$AB = d \sin \theta \quad (2.4)$$

Inserting into equation (2.2):

$$n\lambda = 2d \sin \theta \quad (2.5)$$

Here n is an integer, λ is the wavelength of the incoming x-rays, d is the interplanar spacing between successive atomic planes and θ is the angle between incident x-ray beam and surface of film, which should be equal to the angle of reflection [26].

The grain size was calculated from Scherer's formula [27]:

$$D = \frac{0.94 \lambda}{\beta \cos \theta} \quad (2.6)$$

2.3 Optical properties of metal oxide

Light reflected from the different interfaces of thin films can be in phase or out of phase. It produces constructive (adding intensities) interface patterns or destructive (subtracting intensities). These intensities can be written in the following relation [28]:

$$I_0 = I_A + I_R + I_T + I_S \quad (2.7)$$

Where I_0 is the intensity of incident light beam, I_A is the absorbed intensity, I_T is the transmitted intensity, I_R is the reflected intensity and I_S is the scattered intensity as shown in Fig.2.2.

The coefficients for absorbance ($A = I_A/I_0$), reflectance ($R = I_R/I_0$), transmittance ($T = I_T/I_0$), and scattering ($S = I_S/I_0$), equation (2.7) can be reedited,

$$A + R + T + S = 1 \quad (2.8)$$

Because the scattering part is very small, equation (2.8) is rewritten as:

$$A + R + T = 1 \quad (2.9)$$

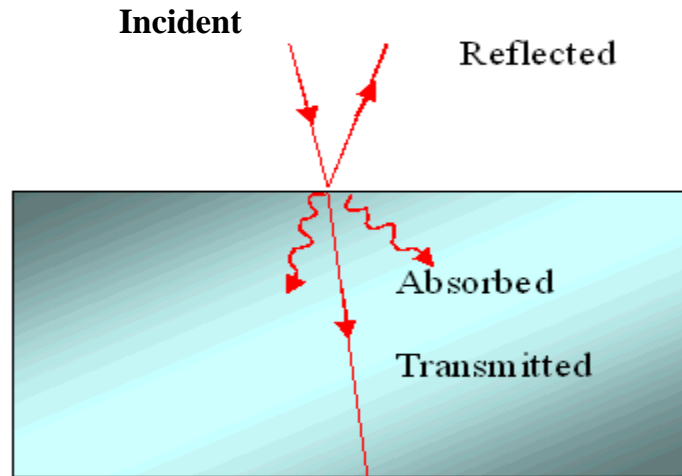


Figure 2.2: Light reflectance, transmittance and absorbance

2.3.1 Absorption of light in matter

Absorption depends on the state of electrons in materials. All electrons are known to vibrate at their natural frequency (specific frequencies). The electrons of the atom will become excited and set into a natural vibrational motion when light (photons) interacts with that atom with the same natural frequency. The electrons of the atom interact with neighboring atoms during vibration and convert this vibrational energy into thermal energy. The intensity of the photon flux decreases exponentially with distance through the semiconductor according to the following equation [29]:

$$I_T = I_0 \exp(-\alpha d) \quad (2.9)$$

we can obtain absorption coefficient (α) :

$$\alpha = \frac{A(2.303)}{d} \quad (2.10)$$

Where $A = \log I_0/I_T$ and represent absorbance, d is the thickness of thin film.

2.3.2 Energy Band gap (E_g)

Electrons in an isolated atom have discrete energy levels, but when atoms are brought together, these degenerate energy levels will split into many levels due to the atomic interaction; the levels may be treated as a continuous band of allowed energy states because they are so closely separated. The two highest energy bands are the valence band and the conduction band. The valence and conduction bands are separated by a region which designates energies that the electrons in the solid cannot possess due to the quantum selection values. This region is called band gap (E_g). Bonds between atoms in a semiconductor are only reasonably strong. Thus thermal vibrations may break some bonds. Then, the electron which is injected from the valence band into the conduction bands is now a mobile negative charge carrier, and the atom from which the electron grows is left with a negative charge deficiency, i.e. a positive net charge, also called a hole. The mechanism is illustrated in Fig 2.3.

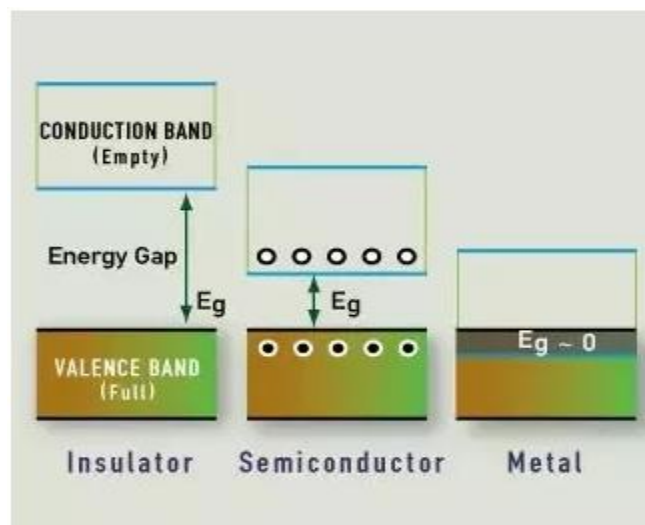


Figure 2.3: Energy band gap of Insulator, Semiconductor and Metal

To find the energy band gap of semiconductor, from absorption coefficient spectra the Tauc's relation is employed [30]:

$$(\alpha E)^{1/p} = A(E - E_g) \quad (2.11)$$

Where: (α) is the absorption coefficient,

$E = h\nu$ (Photon energy), h : Plancks constant.

(p) is a constant related to the optical transition type and takes values of 1/2, 2, 3 or 3/2, where 1/2 refer to direct allowed transitions, 3/2 assigned for direct forbidden transition, 2 indicate indirect allowed transitions and 3 means is indirect forbidden transition.

(A) is a constant determined by transition probability and depend on the material properties,

(E_g) is the energy band gap between valance and conduction band.

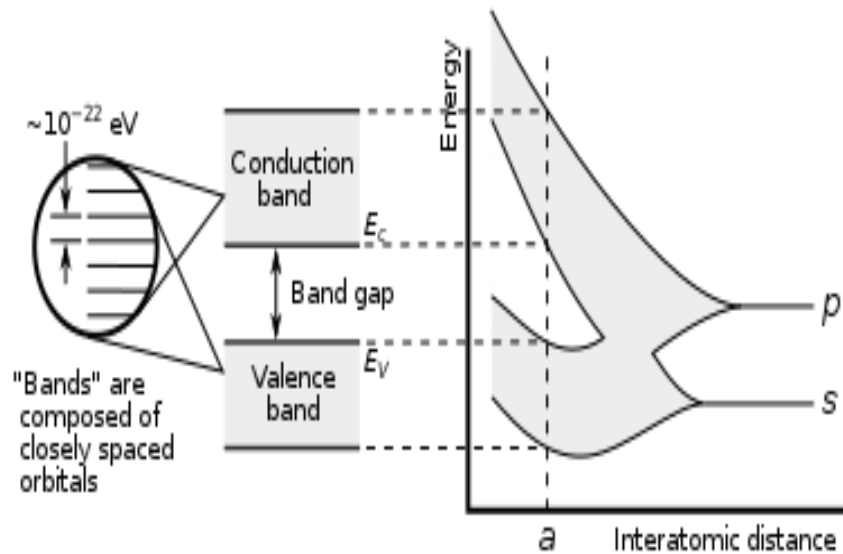


Figure 2.4: Energy band gap diagram.

To derive equation (2.11) , we follow the energy band diagram which is shown in Fig.2.4

$$\text{Initial energy, } E_i = \frac{\hbar^2 k^2}{2m_{eh}^*} \quad (2.12)$$

Where m_{eh}^* is effective mass of electron (e) or hole (h).

$$\text{Final energy, } E_f = h\nu - E_i \quad (2.13)$$

The initial and final energy states of the bands are given by [29]:

$$E_f - E_g = \frac{\hbar^2 k^2}{2m_e^*} \quad (2.14)$$

The electron resides in the valance band up to the conduction band when the incident photons interact with solids, where:

$$E_f = h\nu - |E_i| \quad (2.15)$$

Subtracting E_g from both sides of equation (2.15) we get:

$$E_f - E_g = h\nu - E_g - |E_i| \quad (2.16)$$

Substituting equations 2.13 and 2.14 into (2.16) one obtains:

$$\frac{\hbar^2 k^2}{2m_e^*} = h\nu - E_g - \frac{\hbar^2 k^2}{2m_h^*} \quad (2.17)$$

Rewriting equation (2.17) in another form:

$$h\nu - E_g = \frac{\hbar^2 k^2}{2m_e^*} + \frac{\hbar^2 k^2}{2m_h^*} = \frac{\hbar^2 k^2}{2} \left(\frac{1}{m_e^*} \right) + \left(\frac{1}{m_h^*} \right) \quad (2.18)$$

and recalling that the density of states in an energy spectrum extended from $(h\nu)$ to $(h\nu+d(h\nu))$ have the form [31]:

$$N(h\nu)d(h\nu) = \frac{8\pi k^2 dk}{(2\pi)^3} \quad (2.19)$$

Rewriting equation (2.18) gives,

$$k^2 = \frac{2(h\nu - E_g)}{\hbar^2} m_r \quad (2.20)$$

m_r is the reduced mass of electrons and holes and equal to

$$\frac{1}{m_r} = \left(\frac{1}{m_e^*}\right) + \left(\frac{1}{m_h^*}\right) \quad (2.21)$$

Deriving equation (2.20) with respected to (k) and $(h\nu)$:

$$2kdk = \frac{2m_r}{\hbar^2} d(h\nu) \quad (2.22)$$

Substituting equation (2.20) & (2.22) in equation (2.19) to give:

$$N(h\nu)d(h\nu) = \frac{16\pi(h\nu - E_g)m_r}{\hbar^2(2\pi)^3} dk \quad (2.23)$$

By inserting equation (2.20) and equation (2.22) in equation (2.23) the density of state becomes,

$$N(h\nu)d(h\nu) = \frac{16\pi(h\nu - E_g)}{\hbar^2(2\pi)^3} \frac{m_r^2}{\hbar^2 \left(\frac{\sqrt{(2(h\nu - E_g)m_r)}}{\hbar^2} \right)} d(h\nu) \quad (2.24)$$

Rewrite equation (2.24) in the form:

$$N(h\nu)d(h\nu) = \frac{(2m_r)^{\left(\frac{3}{2}\right)}}{2\pi^2\hbar^3} (h\nu - E_g)^{\frac{1}{2}} d(h\nu) \quad (2.25)$$

Since the absorption coefficient is linearly proportional to the initial and final density of states N_i and N_f , respectively thus,

$$\alpha(h\nu) = A^*(h\nu - E_g)^{1/2} \quad (2.26)$$

$$\text{Where } A^* = \frac{q^2 \left(\frac{2m_h^* m_e^*}{m_h^* + m_e^*} \right)^{\frac{1}{2}}}{nch^2 m_e^*} \quad (2.27)$$

To generalize equation (2.26) rewrite it to become,

$$(aE)^{1/p} = A(E - E_g) \quad (2.28)$$

Where p is a constant related to the optical transition type and takes the values of 1/2, 2, 3 or 3/2, where 1/2 refer to direct allowed transitions, 3/2 assigned for direct forbidden transition, 2 indicate indirect allowed transitions and 3 means is indirect forbidden transition [32].

2.3.3 Energy Band Tail (E_e)

Materials which have localized states that extends in the band gap, display an exponential type of decay in the absorption coefficient spectra. The distribution of the band tail in the energy band gap is shown in Fig.2.5. In the low photon energy range, the spectral dependence of the absorption coefficient (α) and photon energy ($h\nu$) is known as Urbach empirical rule, which is given by the equation [29]:

$$\alpha = \alpha_0 e^{E/E_e} \quad (2.29)$$

Where α_0 is a constant and E_e is energy of the band tail, it is often interpreted as the width of the band tail states due to localized states in the normally band gap that is associated with the amorphous or low crystalline materials. Taking the logarithm of the two sides of the last equation, hence one can get a straight line that reveals the tails width through the equation,

$$\ln(\alpha) = \ln(\alpha_0) + \frac{E}{E_e} \quad (2.30)$$

At different wave length, we can draw $\ln(\alpha)$ versus E , and obtain E_e from $1/\text{slope}$.

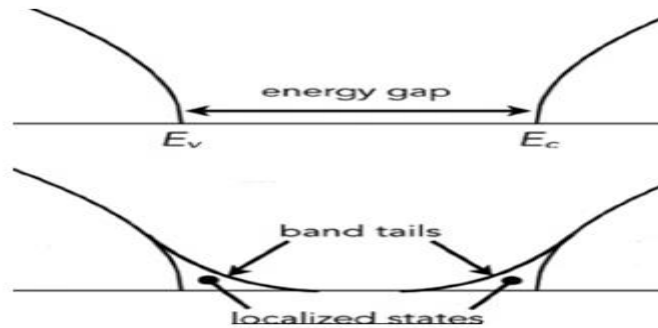


Figure 2.5: Semiconductor band tail structure.

2.3.4 Dielectric Spectra

The refractive index for optical materials is the most important part in dielectric solids. It depends on the wavelength of the incident optical beam. The refractive index- optical wavelength relationship is found by using the dispersion equation [33]:

$$N_{\text{complex}} = n(\lambda) + ik(\lambda) \quad (2.31)$$

Where N_{complex} contain real and imaginary parts of dielectric constant ($\varepsilon_r, \varepsilon_i$), $n(\lambda)$ is refractive index and $k(\lambda)$ is extinction coefficient equals $\frac{\alpha\lambda}{4\pi}$ [34].

The effective dielectric constant ε_{eff} is equal square of the complex refractive index $N(\lambda)$

$$N^2(\lambda) = \varepsilon_{\text{eff}} \quad (2.32)$$

The effective dielectric constant ε_{eff} is expressed in terms of the real (ε_r) and imaginary (ε_{im}) parts where,

$$\varepsilon_{\text{eff}} = \varepsilon_r + i\varepsilon_{im} \quad (2.33)$$

Squaring both sides of equation (2.31), to write the refractive index $N(\lambda)$ in terms of ε_r and ε_{im} :

$$n^2(\lambda) - k^2(\lambda) + i2n(\lambda)k(\lambda) = \varepsilon_r + i\varepsilon_{im} \quad (2.34)$$

By comparing the real and imaginary parts of equation (2.34), we find that :

$$n^2(\lambda) - k^2(\lambda) = \varepsilon_r \quad (2.35)$$

$$2n(\lambda)k(\lambda) = \varepsilon_{im} \quad (2.36)$$

The real and imaginary parts of the dielectric constant as a function of incident wavelength can be written in terms of ϵ_{eff} and α :

$$\epsilon_r = \epsilon_{eff} - \left(\frac{\alpha\lambda}{4\pi}\right)^2 \quad (2.37)$$

$$\epsilon_{im} = \sqrt{\epsilon_{eff}} \left(\frac{\alpha\lambda}{2\pi}\right) \quad (2.38)$$

To derive the effective dielectric constant from the measured transmittance and reflectance we turn the attention to the light interaction with matters.

The reflection coefficient and the normal reflection can be written as:

$$R = \left|\frac{E_2}{E_1}\right|^2 \quad (2.39)$$

From Maxwell's equations:

$$E_2 = \frac{1}{2}E_0(1 - N_{complex}) \quad (2.40)$$

$$E_1 = \frac{1}{2}E_0(1 + N_{complex}) \quad (2.41)$$

Rewrite the normal reflected indicated by equation:

$$R = \left|\frac{1 - N_{complex}}{1 + N_{complex}}\right|^2 = \frac{(1 + n)^2 + k^2}{(1 - n)^2 + k^2} \quad (2.39)$$

We find the reflectance R in terms of effective dielectric constant ε_{eff} and absorption coefficient data α .

$$R = \frac{((\sqrt{\varepsilon_{eff}} - 1)^2 + k^2)}{(\sqrt{\varepsilon_{eff}} + 1)^2 + k^2} \quad (2.40)$$

Where,

$$k = \frac{\alpha\lambda}{4\pi} \quad (2.41)$$

We can rewrite equation (2.40) in the form,

$$R(\sqrt{\varepsilon_{eff}} + 1)^2 + Rk^2 = (\sqrt{\varepsilon_{eff}} - 1)^2 + k^2 \quad (2.42)$$

squaring $(\sqrt{\varepsilon_{eff}} + 1)$ and $(\sqrt{\varepsilon_{eff}} - 1)$ on both sides :

$$R(\varepsilon_{eff} + 2\sqrt{\varepsilon_{eff}} + 1) + Rk^2 = (\varepsilon_{eff} - 2\sqrt{\varepsilon_{eff}} + 1) + k^2$$

$$R\varepsilon_{eff} + 2R\sqrt{\varepsilon_{eff}} + R + Rk^2 = \varepsilon_{eff} - 2\sqrt{\varepsilon_{eff}} + 1 + k^2$$

$$\varepsilon_{eff}(R - 1) + 2\sqrt{\varepsilon_{eff}}(R + 1) + k^2(R - 1) + (R - 1) = 0$$

$$2\sqrt{\varepsilon_{eff}}(R + 1) = -(R - 1)[\varepsilon_{eff} + k^2 + 1]$$

$$\frac{2\sqrt{\varepsilon_{eff}}(R + 1)}{(R - 1)} = -[\varepsilon_{eff} + k^2 + 1]$$

$$\varepsilon_{eff} + \frac{2\sqrt{\varepsilon_{eff}}(R + 1)}{(R - 1)} + k^2 + 1 = 0$$

At high optical wave length λ , k become very large value then the number 1 will be ignored, and the reflectance R is totally 100%, in this case the low value of energy will be reflected, and the rest will enter.

$$\varepsilon_{eff} + \frac{2(R+1)}{(R-1)} + k^2 = 0 \quad (2.43)$$

This equation is solved to find a formula for ε_{eff} :

$$\sqrt{\varepsilon_{eff}} = \frac{-\frac{2(R+1)}{R-1} \pm \sqrt{\left(\frac{2(R+1)}{R-1}\right)^2 - 4k^2}}{2} \quad (2.44)$$

When we look to equation (2.44) we find the two roots involved, these roots are squared and separated in to two solutions:

$$\varepsilon_{eff1} = \left(\frac{-\frac{2(R+1)}{R-1} + \sqrt{\left(\frac{2(R+1)}{R-1}\right)^2 - 4K^2}}{2} \right)^2 \quad (2.45)$$

$$\varepsilon_{eff2} = \left(\frac{-\frac{2(R+1)}{R-1} - \sqrt{\left(\frac{2(R+1)}{R-1}\right)^2 - 4K^2}}{2} \right)^2 \quad (2.46)$$

Lorentz Model for Dielectrics

The Lorentz classical theory is based on the classical theory of interaction between light and matter and is used to describe frequency dependent polarization due to bound charge. The binding between electrons and nucleus are supposed to be similar to that of a mass – spring system. Material polarization is incorporated into the constitutive relations. Drude Lorentz model relates the imaginary part of the dielectric constant with the incident light frequency (ω) by the relation:

$$\epsilon_{im} = \frac{\omega_{pe}^2 \omega}{\tau((\omega_e^2 - \omega^2)^2 + \omega^2 \tau^{-2})} \quad (2.47)$$

Where $\omega_{pe} = \sqrt{4\pi n e^2 / m^*}$, is electron bounded plasma frequency, τ , ω_e , n and m^* are being the free charge carrier scattering time, the resonance frequency, the free charge carrier density, and the free electrons effective mass. The drift mobility of electrons which results from the incident electromagnetic field interaction with the CuO samples may be also estimated from the ϵ_{im} spectra ($\mu = e\tau/m^*$) [35].

Plasmas

In a plasma, however, the electrons in the “cloud” are far enough from each other and from the ionized nuclei that they do not collide, statistically speaking (the plasma has a very small value of mean free collision time) [36]. Plasmon’s is an excitation of collective charge-density fluctuations [37]. Free electrons can efficiently emit or absorb plasmons excited in a thin conductor, giving rise to multiple energy peaks in the transmitted electron spectra separated by multiples of the Plasmon energy [38]. Localized surface Plasmon (LSP) resonances are the oscillations of collective electrons that can be excited by light on

the surfaces of metallic nanostructures. The optical energy is confined to nanoscale volumes by the LSP resonances with potential for high-density integration of optical components [39, 40]. Plasmonic nanodevices are used for performing the second-order spatial derivative of light fields [41].

Chapter Three

Experimental Details

In this chapter, we report the experimental details, procedures, devices and techniques used for measurements. Namely, the thermal vapor deposition technique, the X-ray diffraction technique (XRD), the UV-VIS-NIR spectroscopy technique and annealing processing technique are explained.

3.1 Samples preparation

The glass substrates were ultrasonically cleaned by washing it with water and detergent. Then, the glass substrates were left in H₂O₂ water for 20 minutes at 60° C. The distilled water was shaken in an ultrasonic machine for 20 minutes. We used the cleaned substrate to deposit a 50, 100, 250, 500 and 1000 nm thin films from copper oxide powders by using the thermal vapor deposition system which is shown in Fig.3.1. In this technique material atoms are physically transported one by one from the heated crucible to the substrate [42].

During the deposition we applied the following steps.

- (1) Put the substrate on the substrate holder.
- (2) Close the system, the shutter, vent and chamber.
- (3) Turn on the main power.
- (4) Turn on the roughing pump and wait until the vacuum pressure reaches 10 mbar.
- (5) Turn on the turbo pump molecular and wait until the pressure reaches 10^{-5} mbar.

- (6) Open the water cycling to the thickness monitor.
- (7) Check the connections between the software and the system which is responsible of controlling the thickness monitor.
- (8) Start the evaporation by increasing the current at a slow rate. When material melts, open the shutter and keep the evaporation rate constant.
- (9) When the required thickness is reached, close the shutter and turn off the current.
- (10) Wait for the current system cooling, and then turn off the pumps sequently.
- (11) Wait until the pressure reaches 400 mbar and open the system.

The annealing of films was actualized with the help of an annealing apparatus which is installed in the thermal PVD system shown in Fig.3.1:

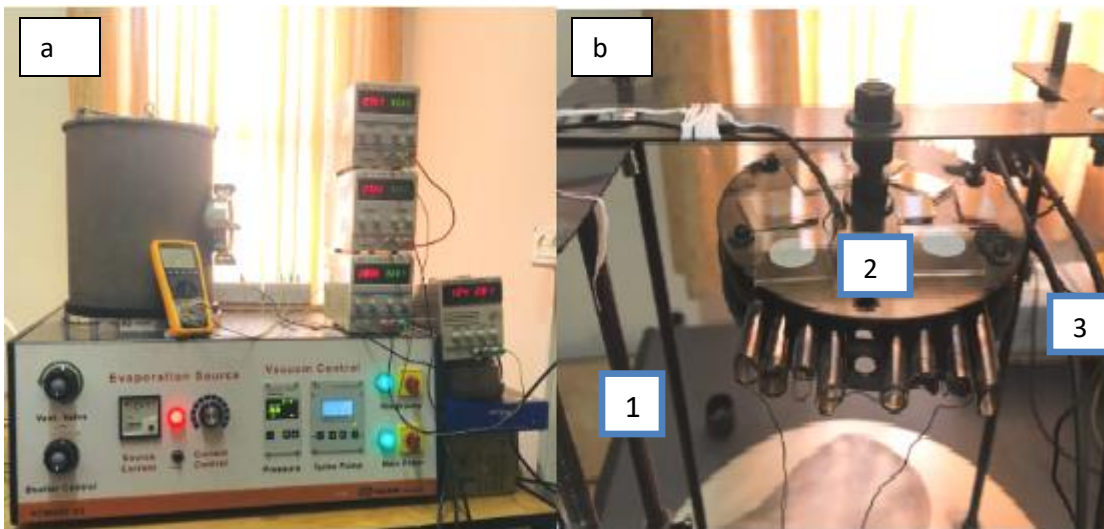


Figure 3.1: a) Thermal evaporation system b) Annealing system, item1 (tungsten), 2 (CuO films) and 3 (thickness monitor)

The annealing system is composed of Nickel-chrome heating wire of 25Ω resistance being installed in glass tubes surrounded by stainless steel plates. The temperature is controlled by K-type thermocouple. The proposed films are annealed at 250°C for one hour under vacuum pressure of 10^{-5} mbar.

Illustrative example of the obtained CuO samples is displayed in Fig 3.2. The obtained films are white yellow colored.

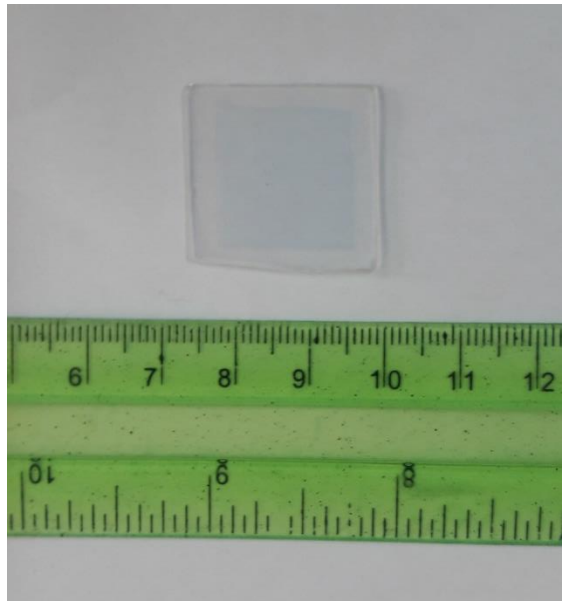


Figure 3.2: Sample of copper oxide thin film (500 nm).

3.2 X-ray diffraction technique

The diffraction principle of the high energy electromagnetic wave is employed to explore the structure of films. Bragg equation is used to describe the diffraction process by

determining the Miller indices of the crystal planes, the lattice constant and crystal structure [43]. When a continuous beam of X-ray is incident on the crystal, the beam reflected from the upper surface travels closer than the one reflected from the lower surface. A constructive interference will occur when the path difference is an integral multiple of the incident wavelength, by applying Bragg's law [42].

XRD measurements were taken using a Rigaku diffractometer with copper anode $K\alpha$ radiation operating at 40 kV and 15 mA in a 2θ range of $10\text{--}70^\circ$ and the 2θ step size of 0.05° and the scan rate was $1^\circ/\text{min}$. The system is composed of a monochromator, a detector, a slit set and a sample holder. The sample rotates by 2θ and the detector collected the intensity of the x-ray beam. Also, the slits are used in order to control the size and shape of the x-ray beam. The data are collected by a software package attached to the system. The schematic of the technique is shown in Fig.3.3. The XRD unit is shown in Fig.3.4.

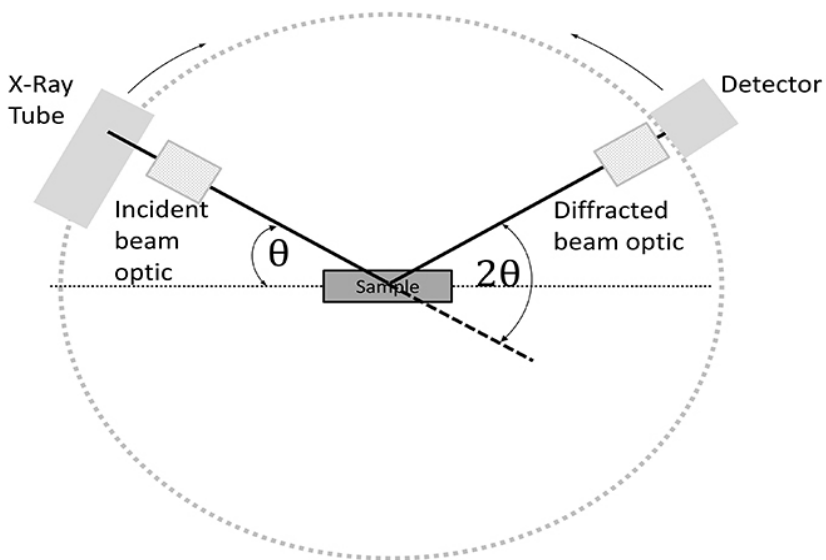


Figure 3.3: Schematic of x-ray diffraction



Figure 3.4: The X-ray diffraction technique (XRD)

3.3. Optical Measurements

The dependence of the optical properties presented by transmittance (T%) and reflectance (R%) were measured in the incident light wavelength range of 300-1100 nm under scan speed of 1200 nm/min on a thermo-scientific evolution 300 spectrophotometer that can be linked with VeeMax II spectrophotometer which is shown in figure 3.5. This system includes wavelengths ranging from UV to the NIR region. The T% and R% spectra are used to determine the absorbability, interband transition, optical energy band gaps, band tails and dielectric dispersion. The data are collected and analyzed by using VISION pro software package.



Figure 3.5: The UV-VIS spectrophotometer.

3.5 “Hot probe” technique

The “Hot probe” technique is a way to know if the semiconductor material is n-type or p-type, by using soldering iron and a standard multimeter. The technique contacting a semiconductor wafer with a “hot” probe such as a heated soldering iron and a “cold” probe. We connected the positive terminal of the meter and the negative terminal to the cold probe. Both probes are sensitive to current meter, if the meter obtain a positive current reading, the material is n-type, if it yields a negative current, it is a p-type semiconductor material. The thermal gradient created and the high-density carriers are generated, which diffused to the lower temperature end of the low carrier density [44]. For an n – type semiconductor, positive voltage created because the electrons diffuse out by concentration

gradient. On the other hand, for a p-type semiconductor negative voltage is generated because holes are excited and diffused out from the hot end to the cold end. Fig3.6 shows the set-up of technique.

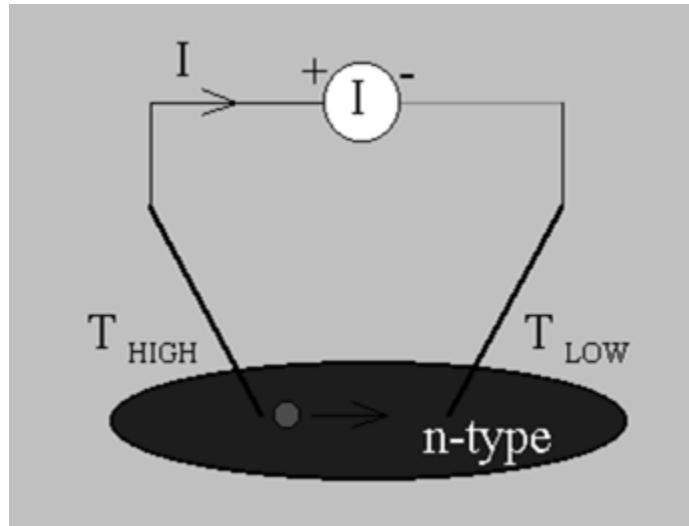


Figure 3.6: Hot probe set-up

Our samples shows negative reading which is mean that the CuO films is p-type as shown in Fig.3.7.

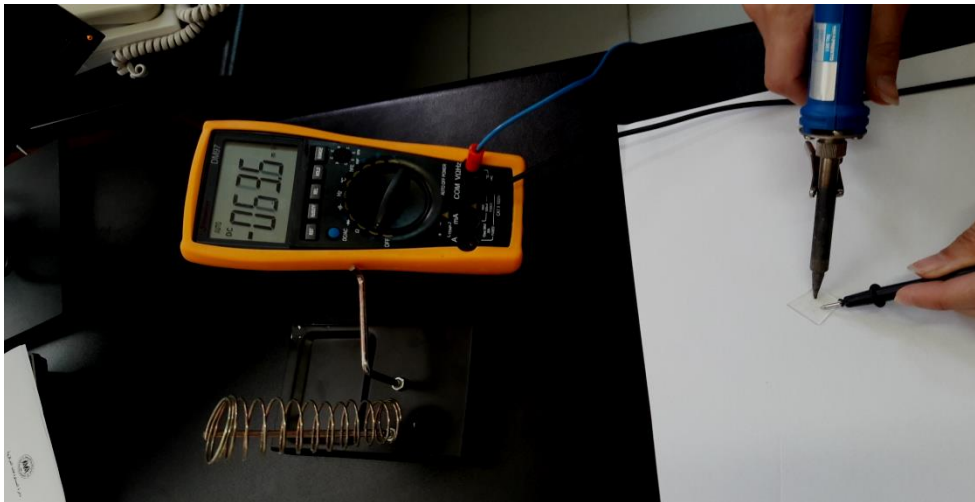


Figure 3.7 : Hot probe result

Chapter Four

Results and Discussion

4.1 Structural properties

The results that arise from the X-ray diffraction measurements on CuO thin films with thicknesses in range 50-1000 nm are discussed in this section. Fig. 4.1 shows the X-ray diffraction patterns for the copper oxide thin films. The figure did not show any intensive peak in all copper oxide films, which means that the copper oxide is amorphous in nature regardless of the film thickness.

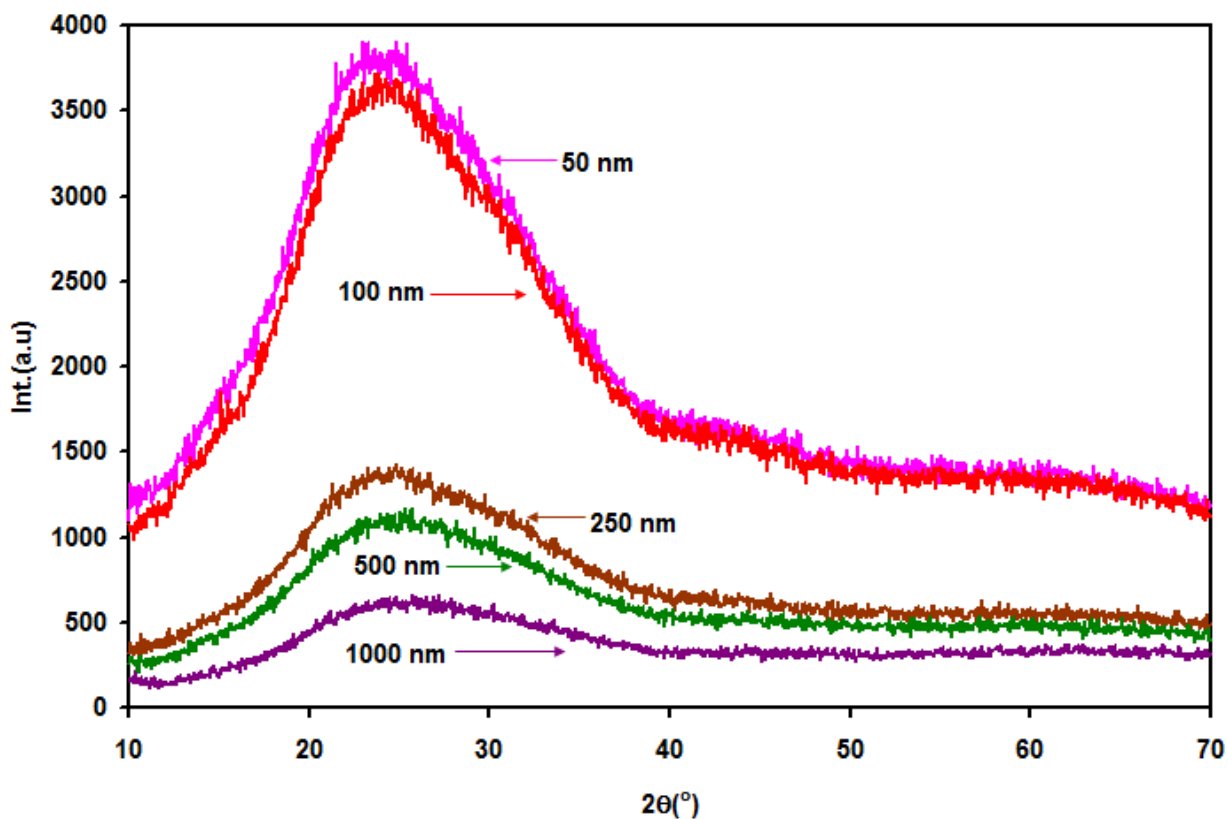


Figure 4.1: XRD patterns of Copper Oxide films measured at room temperature.

The reasons for the amorphous nature of growth of CuO can be investigated from its phase diagram. The calculated phase diagram of CuO revealed preferred growth of copper monoxides phase cubic lattice when grown from melt kept at temperatures below 600°C . In the melt temperature range of $600^{\circ}\text{C} < T < 730^{\circ}\text{C}$ the monoclinic Cu_2O start formation. If the melt temperature exceeds 730°C , the tetragonal Cu_3O_4 appears [45]. However, the tetragonal phase of copper oxide hardly stabilizes. The presence of these three phases at a time in the films causes polymorphic structure and due to the high random orientations of the different types of structures, the amorphous phase becomes preferable.

4.2 Energy dispersive X – ray Spectroscopy (EDS)

To understand the physics beyond the amorphous nature of formation, we have measured the energy dispersive X– ray spectroscopy for CuO films of thickness of 1000 nm. These films were first deposited onto Al substrate to prevent the mixing between the atomic contents of glass and CuO. The spectra are shown in Fig.4.2. Generally, the morphology of the film surface is homogenous. However, some rarely observed rectangular grains which are assigned as point – 2 in Fig.4.2 (a) appeared on the surface. The EDS spectra which were taken from different regions has shown that, the spectrum that appears in Fig.4.2 (b) and (c) contain CuO, Au and Si in its structure. The atomic content measurements reveal the empirical formula $\text{Cu}_{49.50}\text{O}_{50.50}$ for point [1]. Point [2] include SiO_2 as a glass piece on top of film and the $\text{Cu}_{42.31}\text{O}_{57.69}$ and $\text{Cu}_{1.36}\text{O}$.

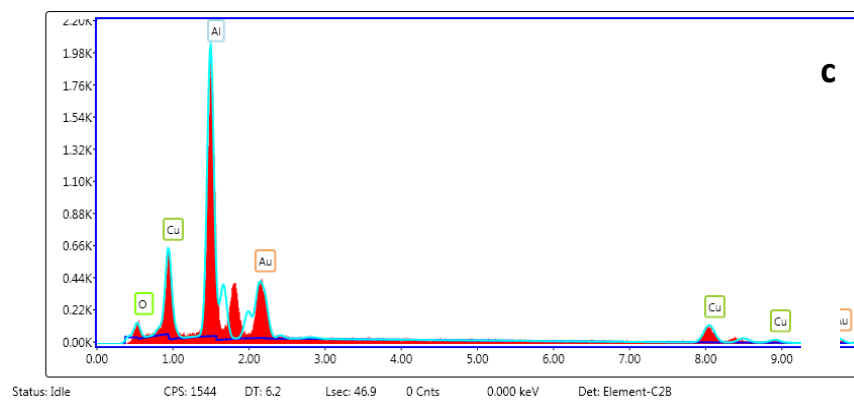
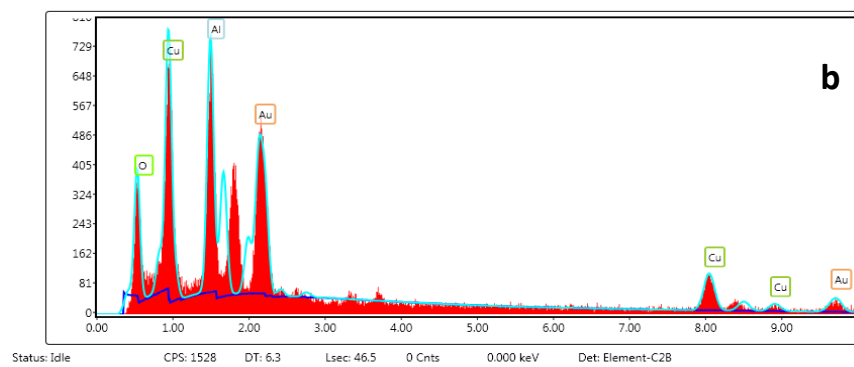
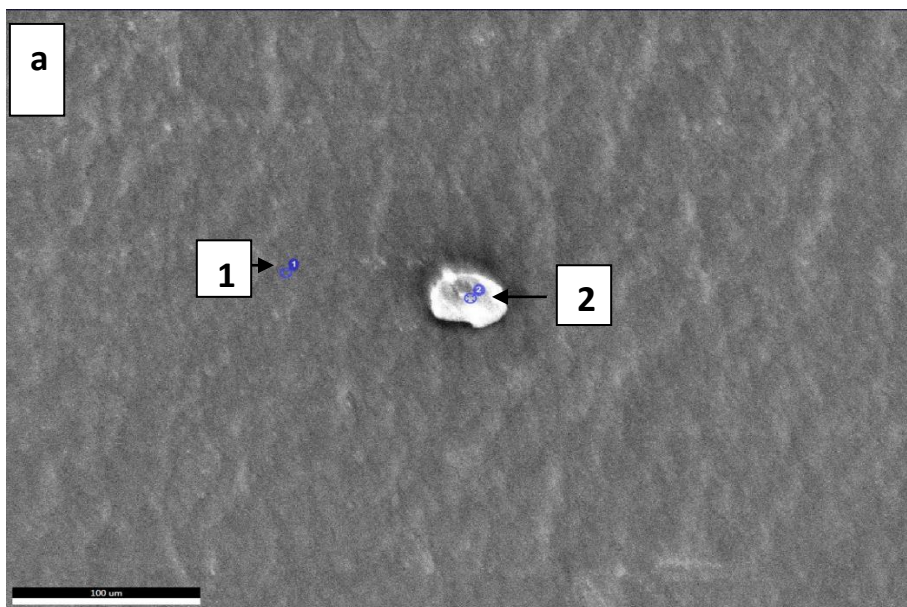


Figure 4.2 (a): SEM image for as grown 1000 nm copper oxide film. (b) and (c) Are the EDS for the as grown 1000 nm copper oxide film from points 1 and 2 respectively appeared in Figure 4.2(a).

Other trials which are not shown in the figure have shown that the films deposited onto glass have high tendency to form Cu_2O_3 and Cu_2O instead of CuO .

The statistical analysis assures the belivements about the reasons for the amorphous nature of growth.

4.3 Optical properties

In order to study the effect of layer thickness on the optical properties of CuO films, the transmittance (T%) and reflectance (R%) of CuO whose thicknesses are 50, 100, 250, 500, and 1000 nm are recorded in the wavelength (λ) range of 300-1100 nm. The thickness of the CuO layers plays a crucial role in the optical properties. The data are presented in Fig (4.3) and Fig.(4.4) respectively. As indicated in Fig.(4.3),the 50 nm film is highly transparent in all range of light spectrum. For the other samples, in the range of 300-900 nm, the transparency decreases with increasing film thicknesses .It is also readable that at a thickness of 50 nm, the transmittance increased with increasing incident light wavelengths in the range of 300-400 nm, then, it remains constant in all the studied range. For samples of thicknesses of 100 nm and 250 nm, the transmittance almost remains constant in all the studied range. On the other hand, for samples of thicknesses of 500 nm, T% spectra show three regions. In the range of 300-530 nm transmittance increased with increasing incident light wavelengths. In the range of 530-700 nm it slightly decreased with increasing incident light wavelengths. In the NIR region, T% remains constant. We noticed that with increasing thickness, the transmittance decreased in visible light region. Also the Fig.4.3 exhibits interference patterns after the thickness exceeds 250 nm and reaches 1000 nm. The transmittance spectra shows oscillatory behavior due to interference between the wave

fronts reflected from the bottom and top surfaces of the thin film. So we can conclude that as the thickness of thin films increases, the interference becomes more pronounced, and the numbers of fringes increased. Such type of films are reported to exhibit a very high electrical conductivity and high visible light transparency with considerable practical applications as solar cells and as other transparent electronics [46].

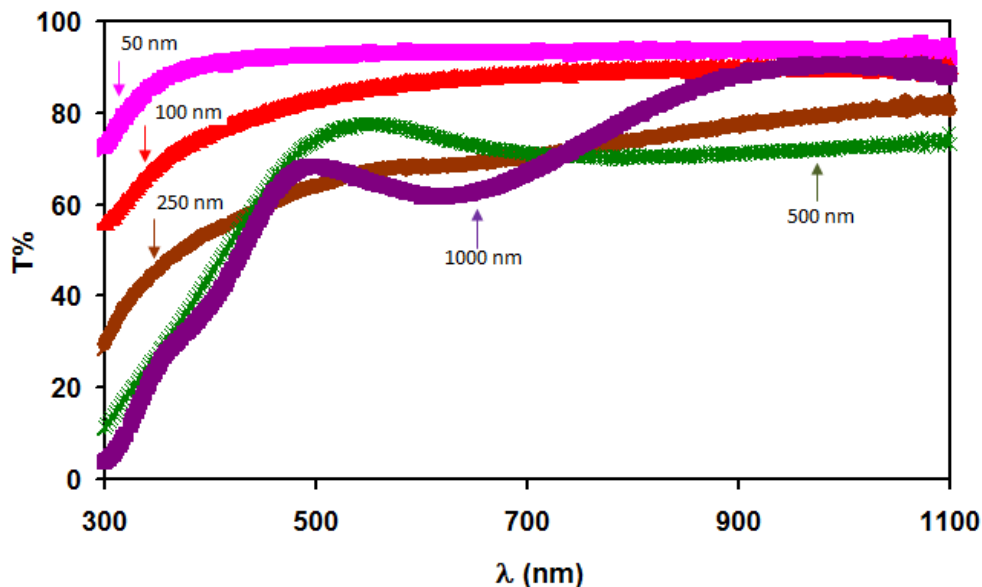


Figure (4.3): Transmission spectra of the CuO thin films measured at 300 K in the wavelength range of 300 to 1100 nm.

On the other hand, the measured reflectance spectra are presented in Fig (4.4). The figure shows an increase in reflectance values with increasing thickness for samples of thicknesses of 50, 100, 250 nm. But it shows different behavior as the thickness is increased to 500 and 1000 nm. The interference becomes more pronounced and deep for thicker films. This behavior can be referred to the morphological and grossness dependent multiple absorption and reflectance caused by the atomic vibrations in the 500 and 1000 nm CuO thin films [47]. The interference between light waves entering to the film with those which are

reflected from the bottom of the film is another reason for the apparent of interference patterns in R% spectra.

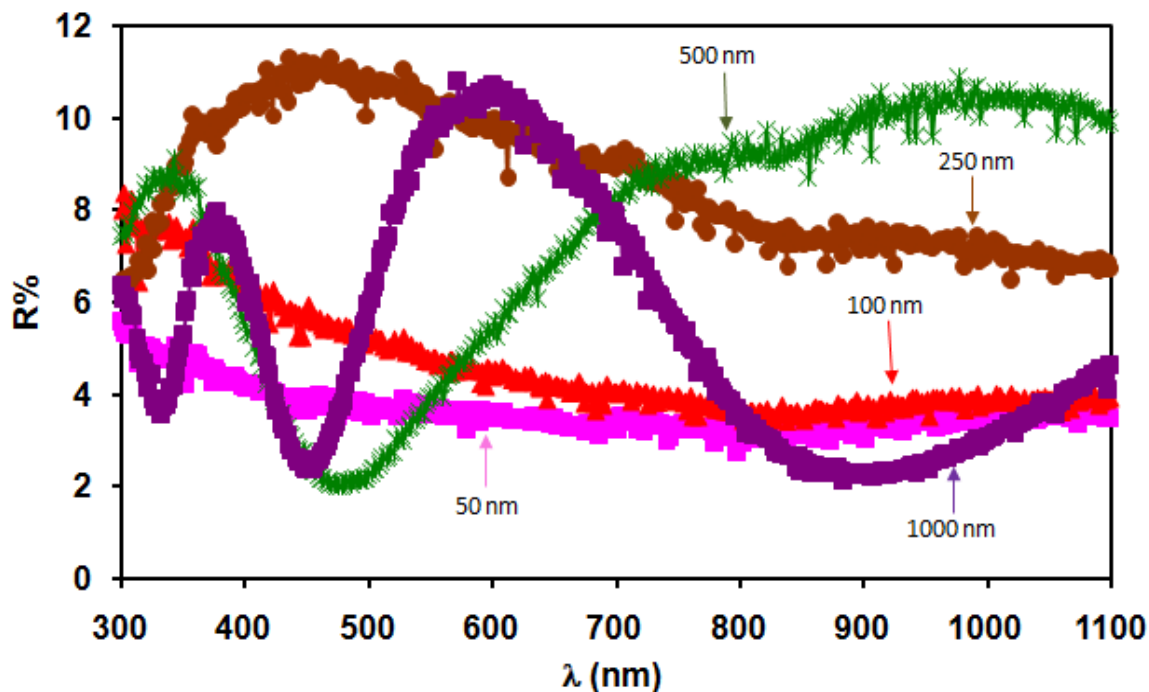


Figure (4.4): Reflection spectra of the CuO thin films measured at 300 K in the wavelength range of 300 to 1100 nm at normal incidence.

We also note that with increasing thickness, the transmittance decreased in visible light region, while reflectance increased. On the other hand, Fig.(4.5) illustrates absorbance spectra for (CuO) films of thicknesses of 50, 100, 250, 500 and 1000 nm. As thickness increase, the absorbance spectra shift up. The absorbance values for all the deposited films, which were calculated from transmittance and reflectance data using the relation $A = 1 - T - R$, are highly dependent on the film thickness.

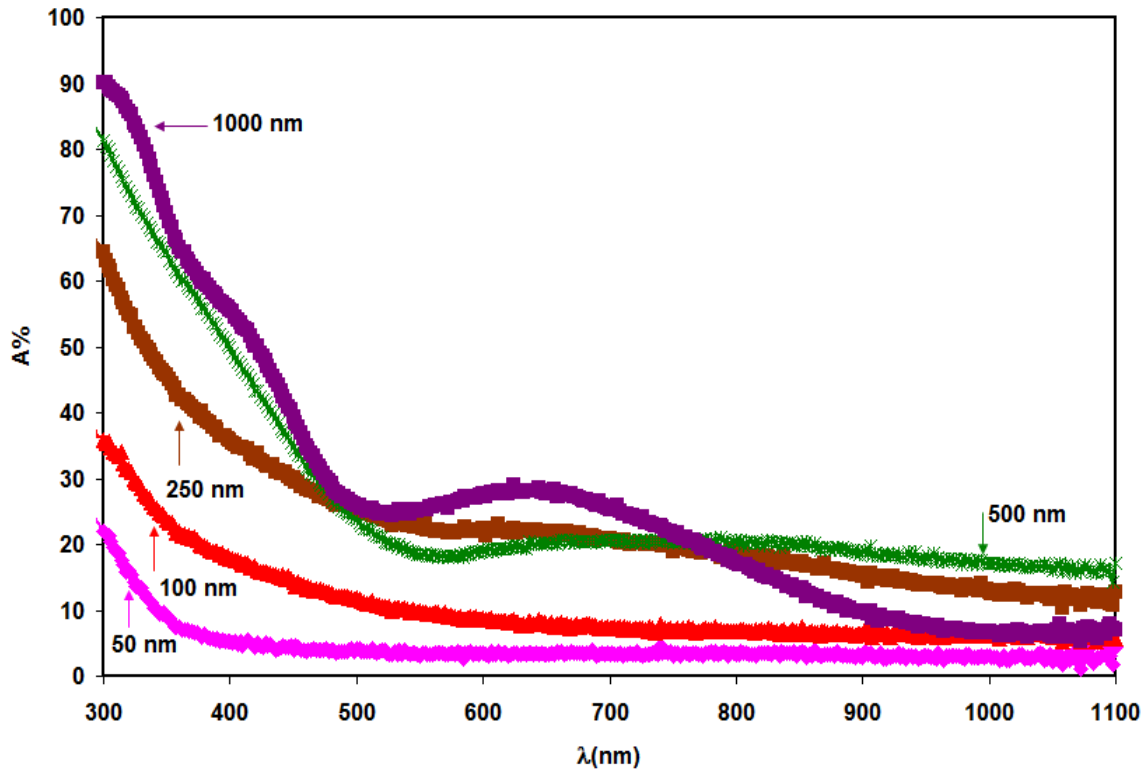


Figure (4.5): Absorbance spectra of the CuO thin films measured at 300 K in the energy range of 1.1 to 4.1 eV.

It is observed from Fig.4.5 that the deposited thin films display high absorbance values in the UV region of the electromagnetic spectrum which remarkably decreased as the incident light wavelength tends towards the near infrared (NIR) region. The non zero absorbance values event in the NIR region indicate the applicability of this material in solar cell technology.

In order to get better understanding of CuO films behavior, we analyzed the absorption coefficient spectra (α). The absorption coefficient values are determined using equation (4.2).

$$\alpha = \frac{A(2.303)}{d} \quad (4.2)$$

Where A is absorbance and d is film thickness, the calculated α values as function of the incident energy E are shown in Fig.4.6. It can be seen that in the spectral range of 4.1 – 3.8 eV, the 50 nm film (Fig.4.6 (a)) have relatively high absorption coefficient compared to thicker samples. According to Tauc and Chopra [48], it is possible to separate three distinct regions in the absorption edge spectrum of semiconductors. The first is the weak absorption region which generally originates from defects and impurities, the second is the exponential edge region, which is strongly related to the structural disorder of the system and the third is the high absorption region that determines the optical energy band gap [49].

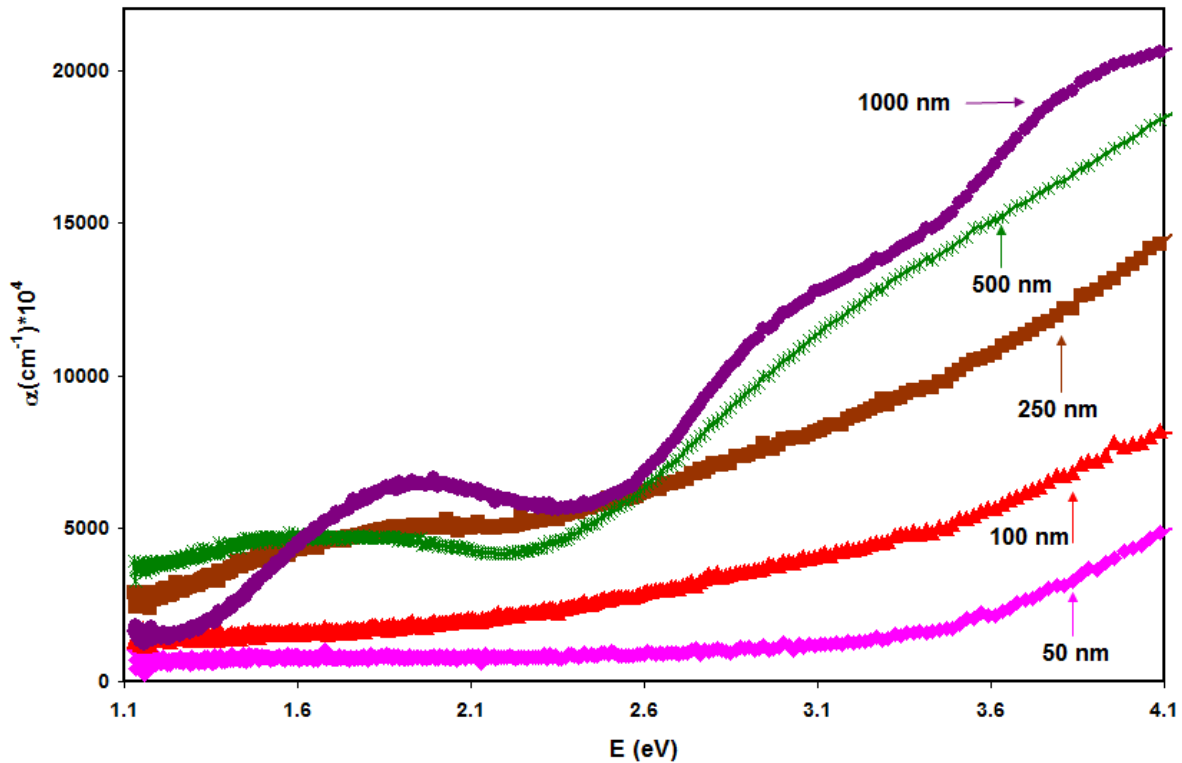


Figure 4.6: Absorption coefficient Vs E of Cupper Oxide thin films.

In general, the absorption coefficient values in the ultraviolet region are larger than those in the visible light region and decreased when NIR region is reached. This behavior may be assigned to the shrinkage of the optical energy band gap [50]. Fig.4.5 shows that the optical absorbance in the UV region and visible light region (VIS) region can be increased by increasing thickness. The absorption coefficient spectral analysis indicates the presence of long and wide band tails of the centered states in the low absorption region [48]. It is also noticeable that the α -spectra for films of 50 nm thick sharply decrease, with decreasing incident photon energy. It exhibit values less than 1000 cm^{-1} as photon energy reaches 3.5 eV. The CuO sample which exhibit thickness of 100 nm follow slower trend of variation. Generally, above 3.0 eV the thicker the film Fig.4.6, the smother the slope of the $\alpha - E$ spectra.

In order to obtain more detailed information about the optical band gap energy (E_g) of the films, the absorption coefficient spectra were analyzed in accordance with Tauc equation (4.3).

$$(\alpha E)^{1/p} = B(E - E_g) \quad (4.3)$$

the respective $(\alpha E)^2$, $(\alpha E)^{2/3}$, $(\alpha E)^{1/2}$, $(\alpha E)^{1/3}$ versus E variations were plotted and compared. The best fit of the data for all samples of thicknesses larger than 100 nm (Fig.4.7(c),(d) and (e)) was obtained for $(\alpha E)^2 - E$ variation indicating that the band gap is of direct allowed transitions type. Our fitting procedure which is based on the linearity that cover the widest possible range of data. From the fittings which is shown in Fig 4.7 (a) and (b) we have observed that films of thicknesses of 50 and 100 nm exhibit an indirect allowed transition type band gap. This behavior could be due to the morphology of the

films which may contain more than one type of composition in its structure. It was reported that the CuO forms valence band states in Cu $3p^6$, $3d^{10}$, $4s^1$, and in oxygen $2s^2$, $2p^4$. The minimum energy splitting between the valence and minimum of conduction band is 2.17 eV for Cu_2O , 2.62 eV for CuO and 1.34 – 1.50 eV for Cu_3O_4 [51]. It is also mentioned that while Cu_2O is a direct band gap semiconductor, CuO of indirect type. In contrast to these types, Cu_3O_4 exhibit both types of energy band gaps. Transitions in CuO take place from Cu $3d_{x-y}$, O $2p$ to Cu $3d_{x-y}$. The three dimensional character of the p – orbital make the indirect transitions more preferable [51]. Since the CuO grow, in amorphous nature. It is possible to think that this material contain more than structural phase in its composition. These structural phases display different optical absorption bands that result in more than one type of energy band gap and more than one band gap in the same film material. The calculated band gaps are shown in table 4.1.

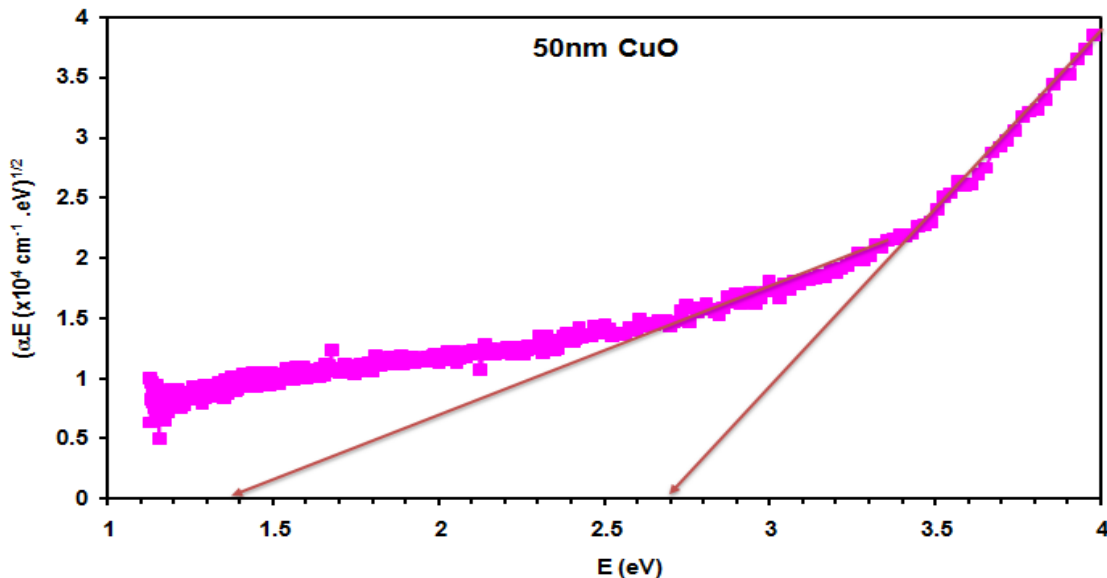


Figure 4.7 (a): Energy band gaps investigation for the 50nm CuO thin films

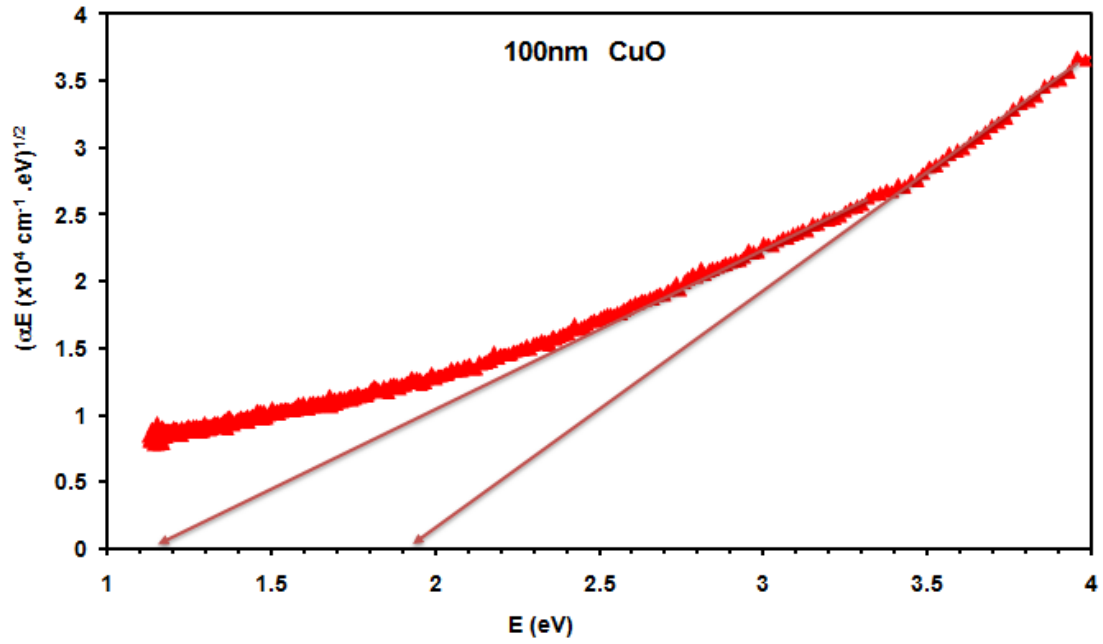


Figure 4.7 (b): Energy band gaps investigation for the 100nm CuO thin films

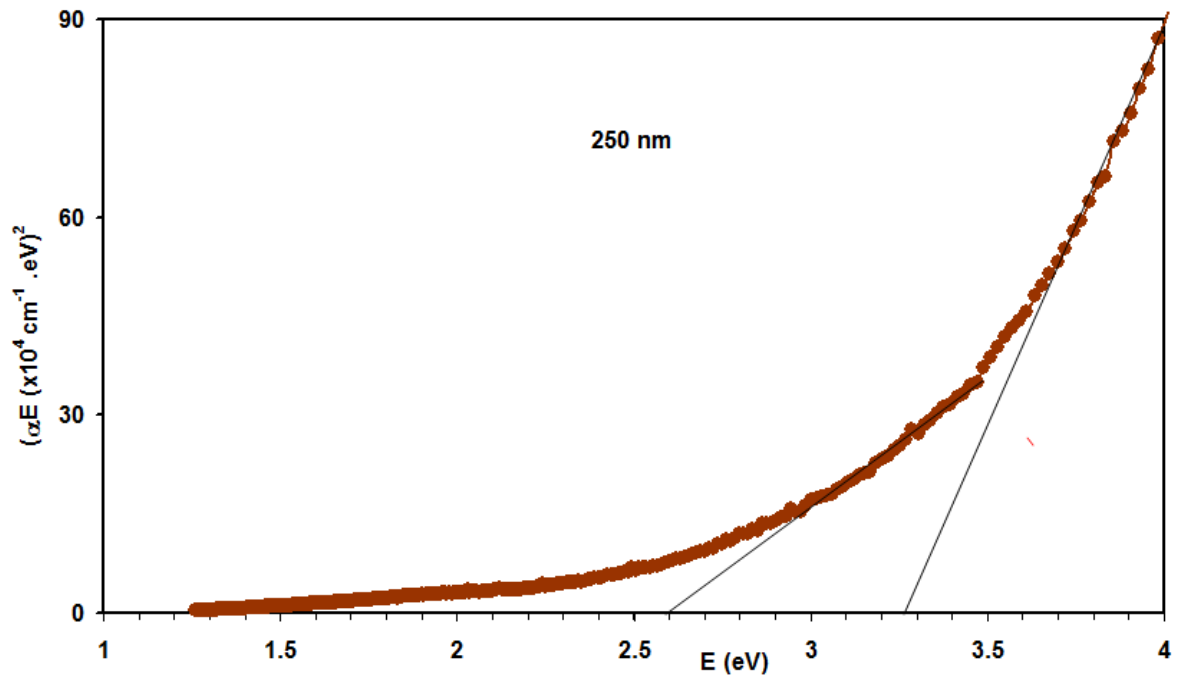


Figure 4.7 (c): Energy band gaps investigation for the 250nm CuO thin films

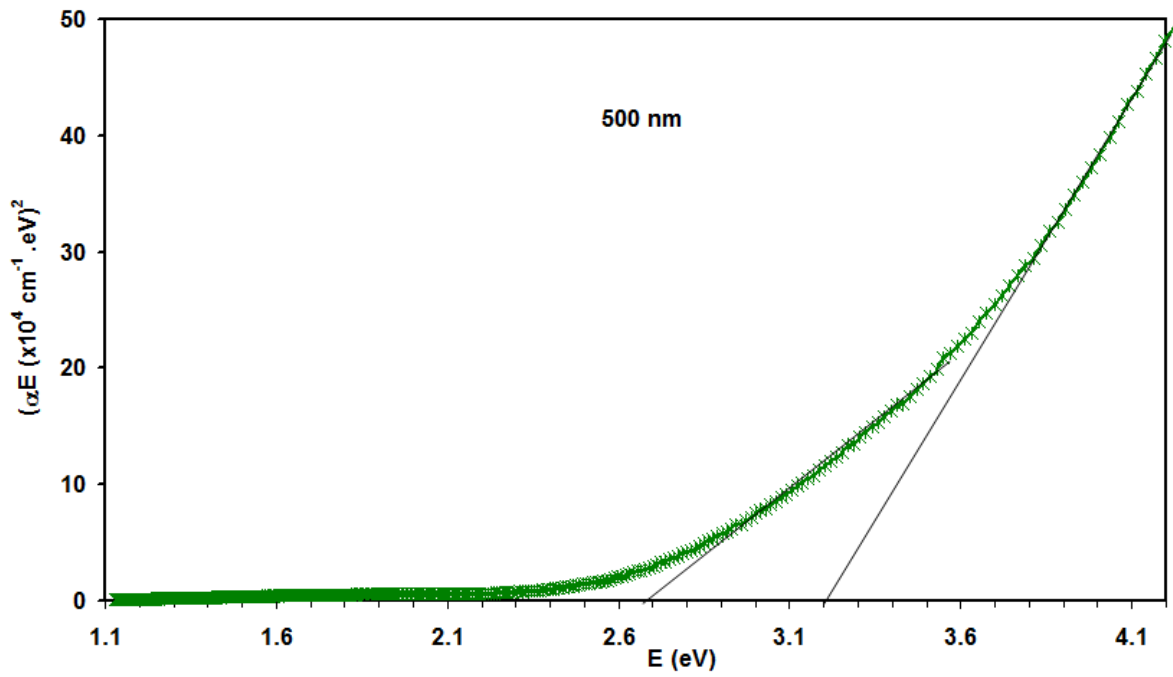


Figure 4.7 (d): Energy band gaps investigation for the 500nm CuO thin films

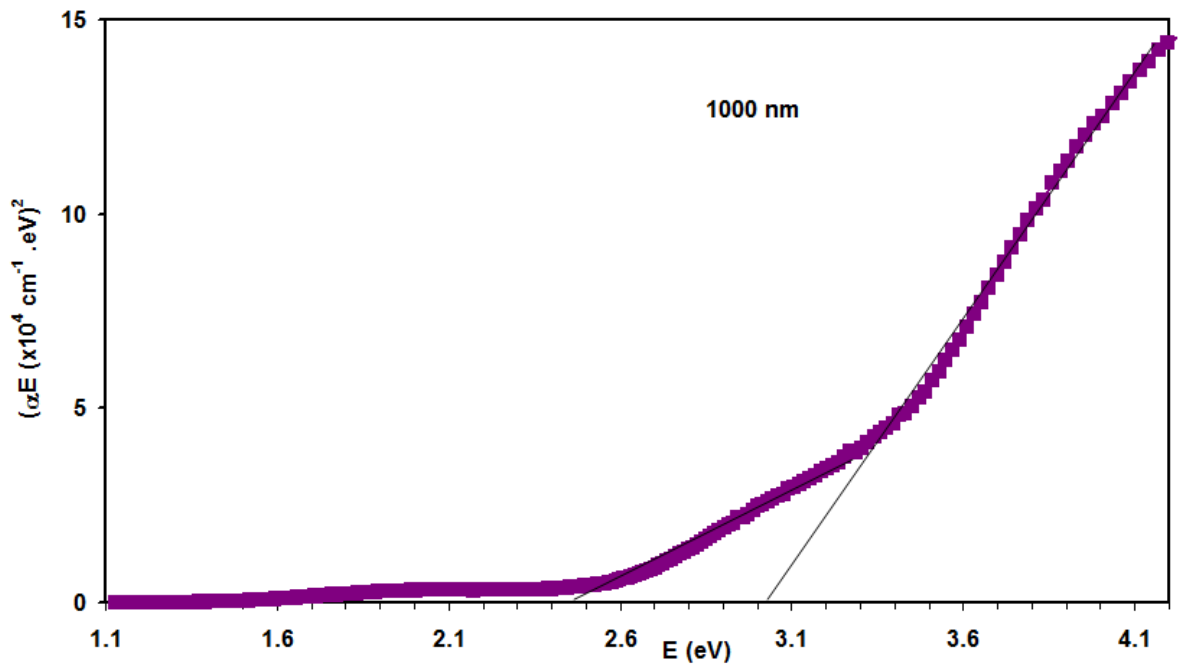


Figure 4.7 (e): Energy band gaps investigation for the 1000nm CuO thin films.

In the low absorption region, semilogarithmic curve fitting was used to obtain the band tail, that is defined as the width of the localized states available in the optical band gap that affects on the optical band gap structure and optical transitions [52]. The band tail is determined by equation (4.4):

$$\ln(\alpha) - \ln(a_0) = \frac{E}{E_e} \quad (4.4)$$

Figure 4.8 shows the variation of $\ln(\alpha)$ versus photon energy for all thicknesses of CuO thin films. The value of band tail were calculated from the slope of the solid best fit lines. The obtained values are given in Table 4.1.

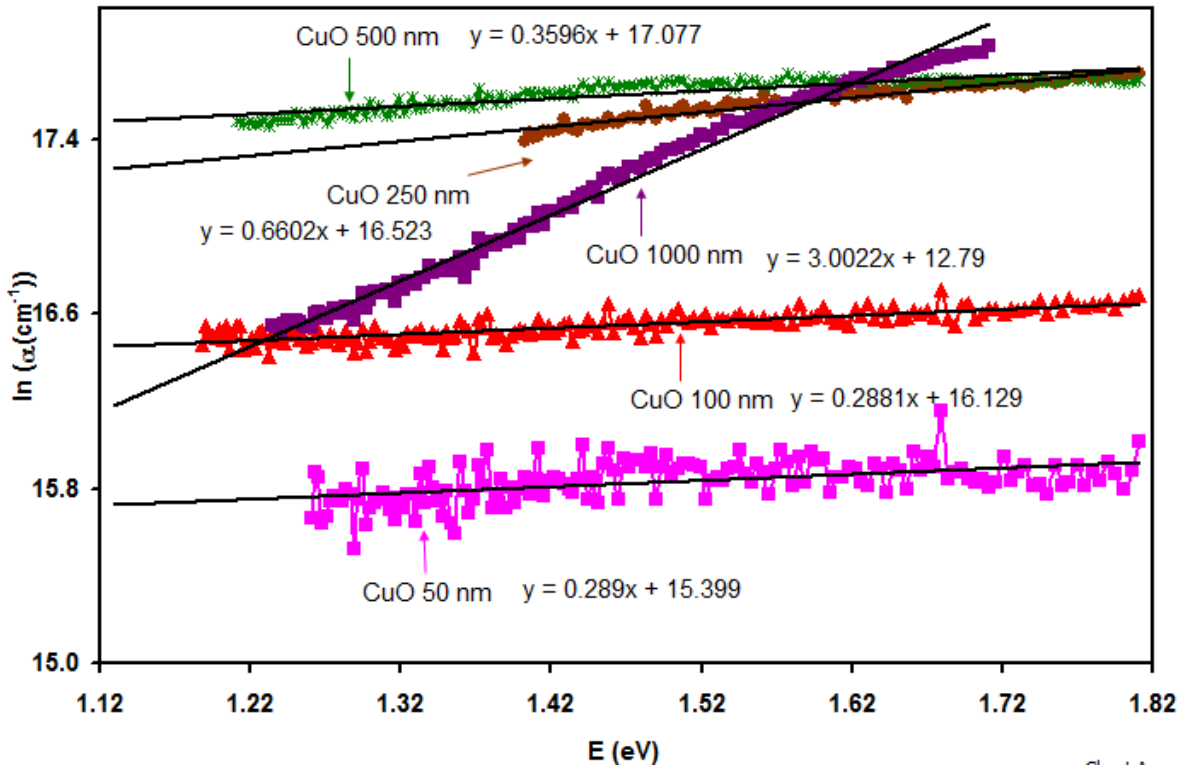


Figure 4.8: $\ln(\alpha) - E$ variation in the low absorption region for band tail investigation of the CuO thin films.

Table (4.1) : The band gaps and band tails of the CuO thin films.

d(nm)	Indirect		Direct		
	50nm	100nm	250nm	500nm	1000nm
E_{g1} (eV)	2.70	1.90	3.26	3.20	3.00
E_{g2} (eV)	1.40	1.10	2.60	2.68	2.50
E_e (eV)	-----	-----	-----	-----	0.33

In accordance with the preceding analysis, the electronic transitions between the valence and conduction bands are found to be direct and indirect - allowed type. For samples of thickness of 50 and 100 nm, the band gap is indirect and it decreases with increasing thickness, but for samples whose thicknesses are 250, 500 and 1000 nm, direct allowed transition type is found. The optical band gap also decreases with increasing thickness. This can be further explained from the three-dimensional quantum size effect leading to a decrease of band gap with increase of particle size, which is well known for colloidal semiconductors [53]. It was observed that increasing the thickness of the films increases the absorbance due to scattering losses. This suggests that the defects in thin films take place during formation of the films [54]. So, as a result of an insufficient number of atoms, unsaturated bonds are being produced [55]. These bonds are responsible for the formation of some defects in the films, and these defects produce localized states in the films. The thicker the film, the wider the localized states in the optical band gap [54], for our

amorphous case, we believe that the extended band tails in the energy band gap is the main reason for the gap attenuate. The thicker the sample, the wide band tail distributions. Such property leads to shrink in the optical band gap we have observed. The shift of absorption edge can be attributed to the difference in grain size or carrier concentration [56]. It had been reported that the absorption edge shifts with the Fermi level to a higher energy in accordance with the formula

$$E_c - E_f = \Delta E_n = \left(\frac{h^2}{8m_c^*}\right) \left(\frac{3}{\pi}\right)^{2/3} n^{2/3} \quad (4.5)$$

With m_c^* being effective mass of electrons in the conduction band and n is the number of charge carriers in the conduction band [57]. Since the density of localized states in the conduction band increases with increasing thickness, the band gap shrunk by an amount of ΔE_n .

On the other hand, the energy band tail must be equal or less than energy band gap over two ($E_e \leq E_g/2$) so we can conclude that the 1000 nm film, have no band tail.

4.4 Dielectric dispersion

The dielectric dispersion properties of the studied films are calculated from the reflectance and absorption coefficient data with help of the previously described equations in the preceding chapters. The real (ϵ_r) equ.(2.37) and imaginary (ϵ_{im}) equ.(2.38) components of the effective dielectric constant are determined to obtain detailed information about optical signal quality and dispersion within the films. Fig.4.9 displays the real part of the dielectric spectra. The figure illustrates thickness effect on the shape of the dielectric spectra.

Particularly, for films of thicknesses of 50 and 100 nm, the dielectric constant values linearly increases with increasing incident photon energy. When the CuO film thickness reaches 250 nm, the nonlinear trend of variation appears. The dielectric constant values exhibit a change in the trend of variation upon energy increasing at 2.80 eV. Further increase in the film thickness to 500 nm caused a minimum in the dielectric spectra at 2.55 eV. On the other hand, duplicating the thickness (1000 nm) make ϵ_r spectra exhibit three minima at 1.39, 2.72 and 1.24 eV. Two resonating peaks of maximum dielectric constant value are also observed at 2.11 and 3.30 eV. The Energy band gap of Cu₂O is 2.1 – 2.38 eV, defective Cu₂O is reported to reveal resonance peak due to oxygen vacancy which oscillate at 1.39 eV [58]. The value of resonance energy being 3.30 eV is assigned as optical gap for CuO phase [59]. The value of energy being 2.7 eV was observed for the transition in the conduction band of Cu. The conduction band in Cu changes to half width from 2.7 eV to 3.2 eV when interfaced with CuO to form tetragonal phase [60]. The value of energy being 1.24 eV is also assigned to the oscillation of O atom against Cu through direct transition in the three dimensional p – states [61].

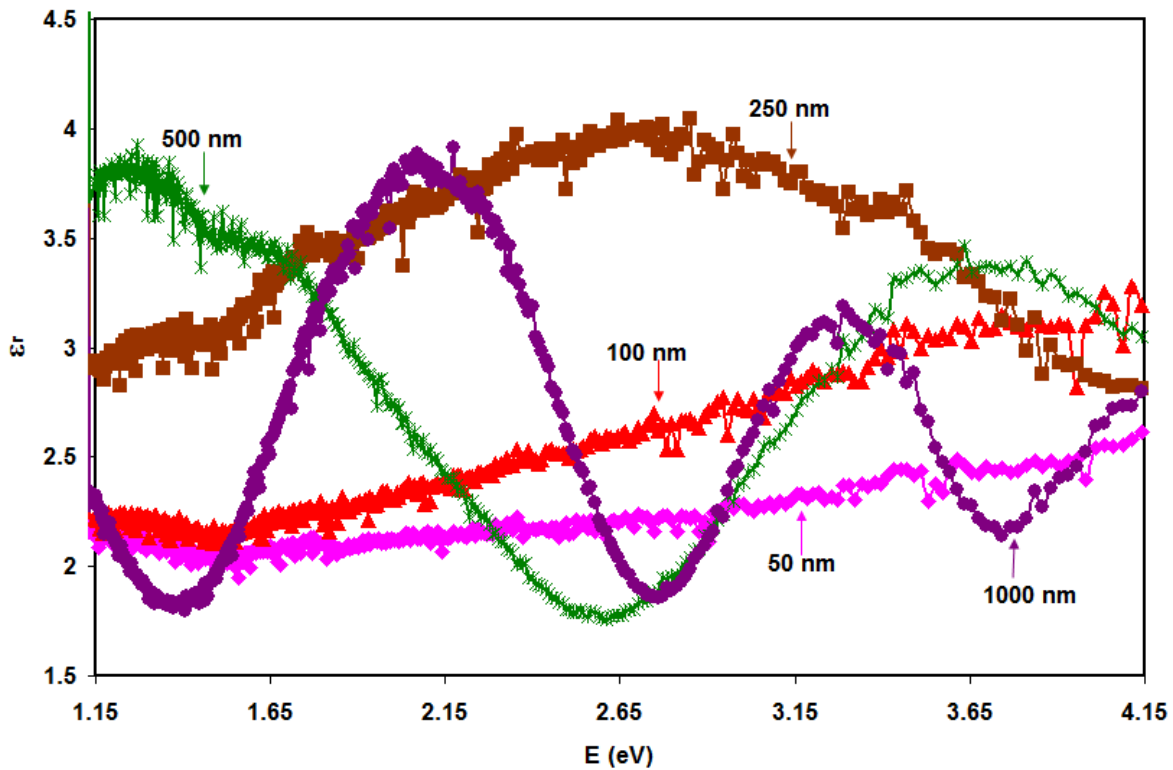


Figure 4.9: Real parts of the dielectric constant of the films measured with energy

The imaginary part of the dielectric constant which is shown in Fig.4.10 can be used to provide information about the optical parameters. As seen, the 1000 nm thick film exhibits two resonating peaks centered at 850 THz (3.52 eV) and 480 THz (1.99 eV). Films whose thickness is 500 nm has also two resonating peaks centered at 840 THz (3.47 eV) and 355 THz (1.47 eV). The frequency response of many materials can be described by using Drude Lorentz model, it usually shows strong dispersion around the resonant frequency [62]. This model is chosen to investigate the advantages of the films as optical conductors [63]. Drude Lorentz model relates the imaginary part of the dielectric constant with the incident light frequency (ω) by the relation [62],

$$\epsilon_{im} = \frac{\omega_{pe}^2 \omega}{\tau((\omega_e^2 - \omega^2)^2 + \omega^2 \tau^{-2})} \quad (4.7)$$

This equation provides information about single resonating peak of the dielectric constant. For coupled resonance ϵ_{im} is obtained through the programming of the equation assuming generalized form of Lorentz model (Lorentz –Drude model).

$$\epsilon_{im} = \sum_{i=1}^k \frac{\omega_{pei}^2 \omega}{\tau_i ((\omega_{ei}^2 - \omega^2)^2 + \omega^2 \tau_i^{-2})} \quad (4.8)$$

The model is based on treating electrons as damped harmonically bound particles subject to external electric fields [64].

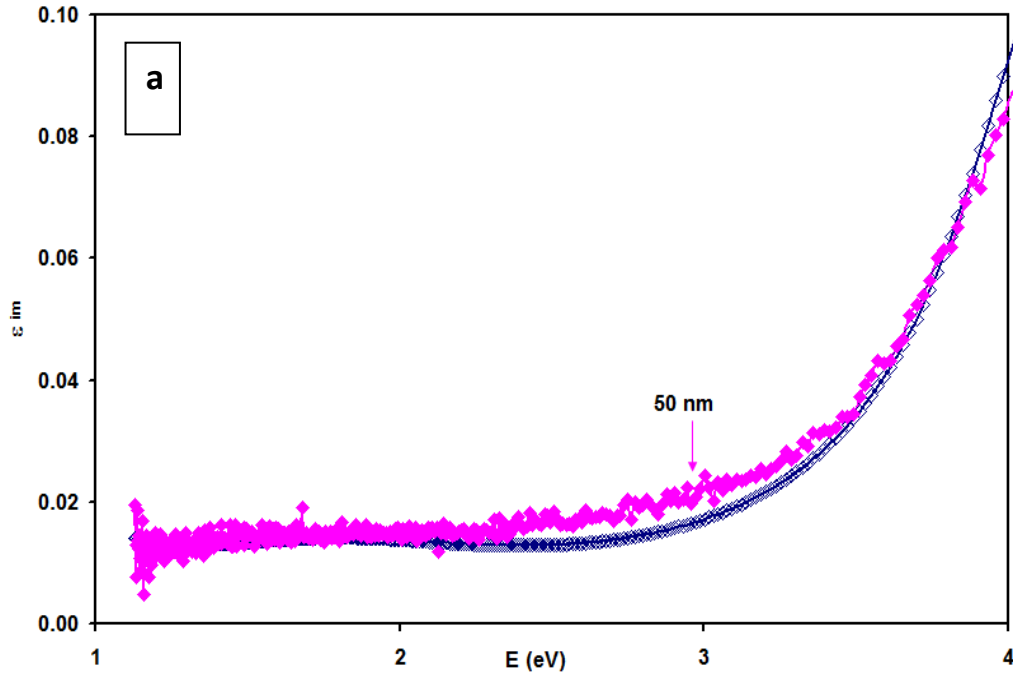


Figure 4.10 (a): Imaginary part of the dielectric constant of the 50 nm CuO film measured in the frequency range of 300-1000 THz.

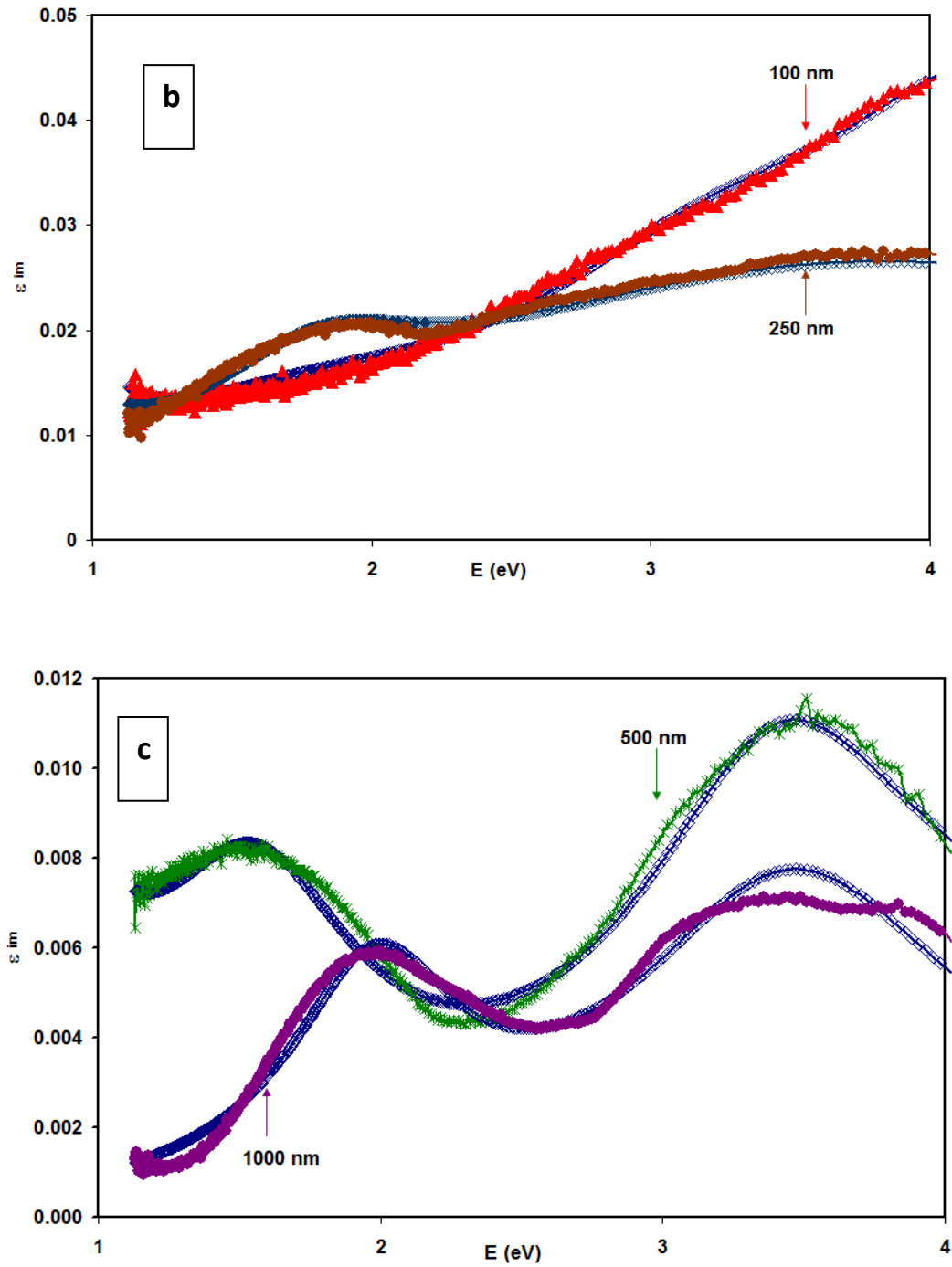


Figure 4.10 (a): Imaginary part of the dielectric constant of the 50 nm CuO film measured in the frequency range of 300-1000 THz. (b) for 100 nm and 250 nm, and (c) for 500 nm and 1000 nm.

Table 4.2 reports the results of the Drude – Lorentz modeling of the imaginary part of the dielectric spectra for the studied films. In accordance with the table, for samples of thicknesses of 50 nm and 100 nm, where the electronic transitions are indirect type, the scattering time (τ), the free hole density (n), the drift mobility (μ), the dc conductivity (σ) and the Plasmon frequency (ω_{pei}) all decreased with increasing thickness, the decrease in the optical conductivity parameters for the two samples may be assigned to the increased random distribution of grain in the amorphous sea. Namely, with increasing thickness, the amount of randomly distributed atoms increases. As the material become denser, the probability of random collisions becomes more pronounced and the free holes are lost due to the random collisions. It is expected that since the increased thickness shrunk the energy band gap, and increased the optical absorbability, the optical conductivity was expected to increase [65]. However, as the table shows, the optical conductivity decreases. One possible reason for this action is the strong recombination of the free holes of CuO with the unbounded atoms at the surface of the films. In this case the number of free carriers available for conduction abruptly decreases. The sudden decrease in the free hole density attenuate all the other optical parameters.

In cesium oxide the increase of cobalt impurities was observed to induce the formation of new recombination centers which led to optical conductivity decreasing [66]. The same behavior can be accepted for our observation. On the other hand, for the samples which exhibit direct allowed transitions, increasing the thickness increases the scattering time and drift mobility as well. These two parameters indicate that a less electronic friction has take place in the samples owing to larger thickness values. This behavior may be assigned to the

external energy provided for the electron as a result of the no need for phonon assistance to reach the conduction band. The higher the kinetic energy of electrons, the shorter longer the scattering time as the holes can move longer distances.

The conductivity provides a measure of how fast an electron can flow through a material, it is defined as [67]:

$$\sigma = nq\mu$$

Where q is the charge and μ is the carrier mobility in the medium and n is the charge carrier concentration/density. Also, $\sigma = \frac{\epsilon_{im} \times w}{2\pi}$, increasing thickness lead to decreasing in imaginary part of dielectric constant so decreasing in conductivity .

d(nm)	50				100				250				500				1000			
i	1	2	3	4	1	2	3	4	1	2	3	4	1	2	3	4	1	2	3	4
τ_i (fs)	3.00	0.40	1.00	0.50	1.00	0.70	0.30	0.50	0.50	0.50	0.20	0.40	0.65	0.73	0.55	0.27	0.90	0.50	0.50	0.27
$W_{ei} (\times 10^{15} Hz)$	1.00	2.90	6.30	6.50	1.50	2.90	5.25	6.50	2.90	4.80	6.00	7.00	1.50	2.48	5.25	6.50	3.05	5.10	5.40	6.30
$n (\times 10^{17} cm^{-3})$	1.00	1.50	8.60	13.00	0.40	0.50	9.00	9.0	1.80	3.00	5.00	7.00	0.25	0.43	1.50	2.5	0.35	0.40	1.00	1.00
$\mu (cm^2/vs)$	59.27	7.90	19.75	9.88	19.76	13.83	5.93	9.88	9.88	9.88	3.95	7.90	12.84	14.42	10.87	5.83	17.8	9.90	9.90	5.30
$\sigma_{DC} = (n \times \mu)q$	0.95	18.96	271.8	205.5	0.13	11.06	85.39	142.3	0.28	47.4	31.6	88.48	0.05	9.92	26.09	21.32	0.099	6.34	15.84	8.48
W_{pei} (GHz)	0.63	0.77	1.85	2.27	0.40	0.45	1.89	1.89	0.85	1.09	1.41	1.67	0.32	0.41	0.77	0.99	0.37	0.40	0.63	0.63

Table 4.2 : The computed parameters of the Plasmon-electron interactions in the CuO thin films.

In the table 4.2, the symbol (i) indicates the number of oscillation, for (i=1) the main oscillator is leader, and it the most important oscillator.

4.5 Annealing process

In an attempt to improve the optical properties through converting the structure of CuO films to polycrystalline, the films were annealed at 250 °C for one hour in vacuum media.

4.5.1 Structural properties

In accordance with Fig.4.11, annealing the samples successfully converted it to polycrystalline. As seen in Fig.4.11, the 250, 500, and 1000 nm samples exhibit peaks at 27.85° , 28.05° and 28.10° respectively. These peaks become clearer and sharper when thickness increases. Table 4.3 shows the effect of sample thickness on the peak position and broadening. Although the number of observed peaks for a particular sample is insufficient to optimize a real solution for the possible structural phases, but the observed peak is still comparable with the literature data. The position of the observed peak suggests that it is assigned to cubic phase of the Cu_2O . Studies on single crystalline CuO nanowires have shown that the peak reflections near 28° relate Cu_2O with plane orientation in the (110) reflection direction [68]. The calculated grain size which is also tabulated in table 4.3 increased with increasing films thicknesses. The increase in the grain size with increasing thickness as a result of the annealing process can be explained in the light of the previously reported literature data on similar materials. Works on ZnO assigned the increase in the grain size to the increased roughness [69]. The roughness is reported to increase the tensile stress [70] which affects the lattice parameters

Table 4.3: The analysis of X-ray measurement

Thickness	2θ	Intensity(w/m^2)	β (rad) $\times 10^{-3}$	D(grain size)nm
250 nm	27.85°	1748	1.744	85.52
500 nm	28.05°	1459	1.570	95.07
1000 nm	28.1°	1523	1.099	135.82

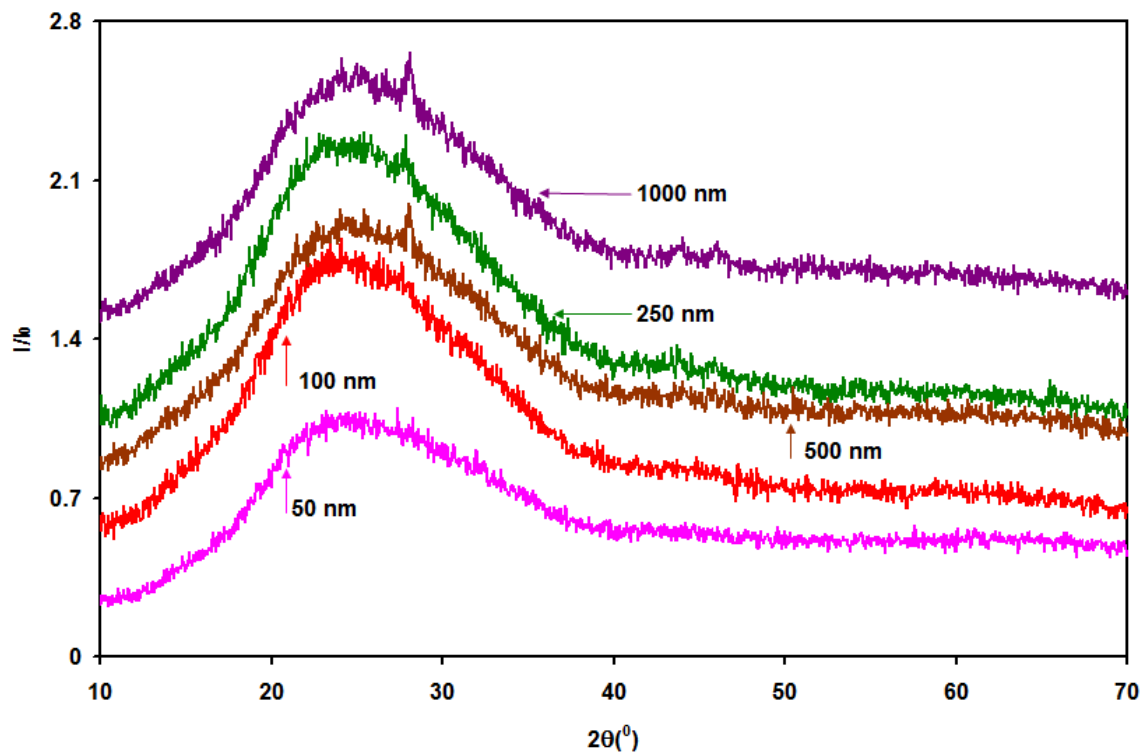


Figure 4.11: XRD patterns of Copper Oxide films annealed at 250°C by using evaporation system

4.5.2 Optical properties

In order to study the effect of temperature on optical properties of copper oxide thin films, the transmittance T% and reflectance R% of 1000 nm CuO were recorded in the wavelength (λ) range of 300-1000 nm thick after annealing the samples at 250 °C . As seen in Fig 4.12, the value of the optical transmission of the annealed samples are less than those of the as grown. The T% values mostly decreases upon annealing, due to the increased roughness that is associated with crystallinity of the films.

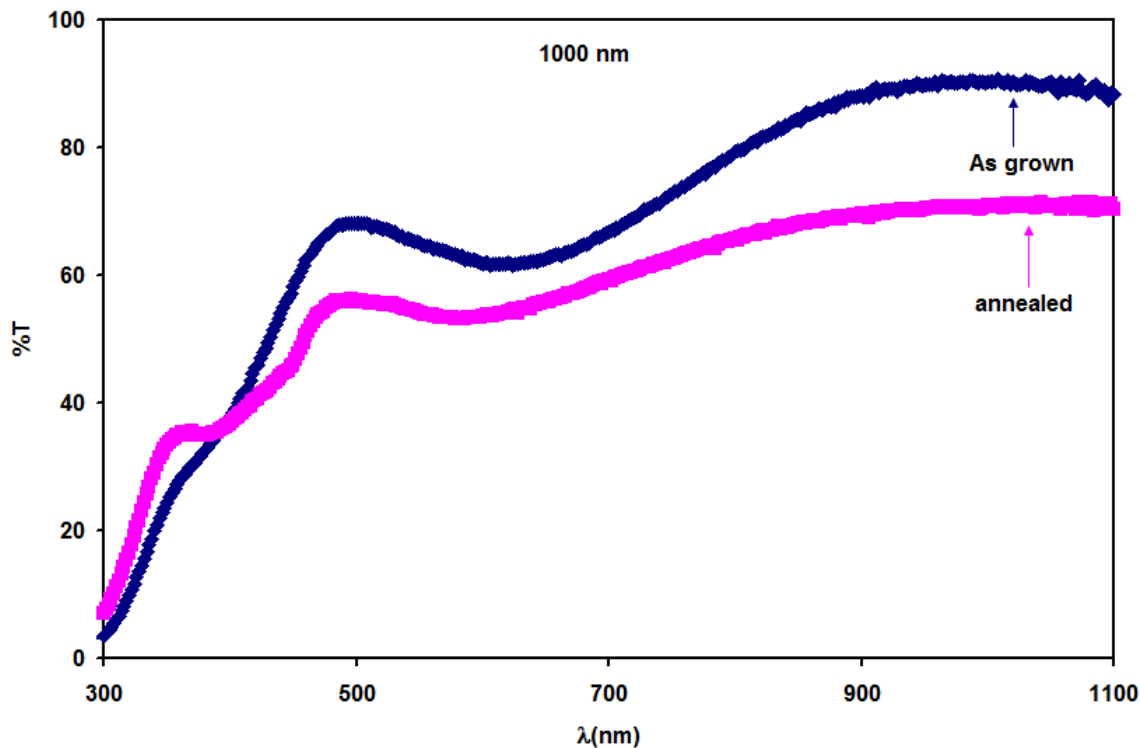


Figure 4.12: Transmission spectra of the CuO thin films as grown and annealed at 250 °C in the wavelength range of 300 to 1100 nm.

It can be observed that, curve of the 1000 nm thick sample exhibit interference fringes with more pronounced peak at 360 nm.

On the other hand, the reflectance decreased upon annealing as shown in Fig.4.13. Since the surface roughness is inversely proportional to the reflection coefficient, the presented spectra can be regarded as a confirmation of the belief that the roughness caused the reduction in the transparency.

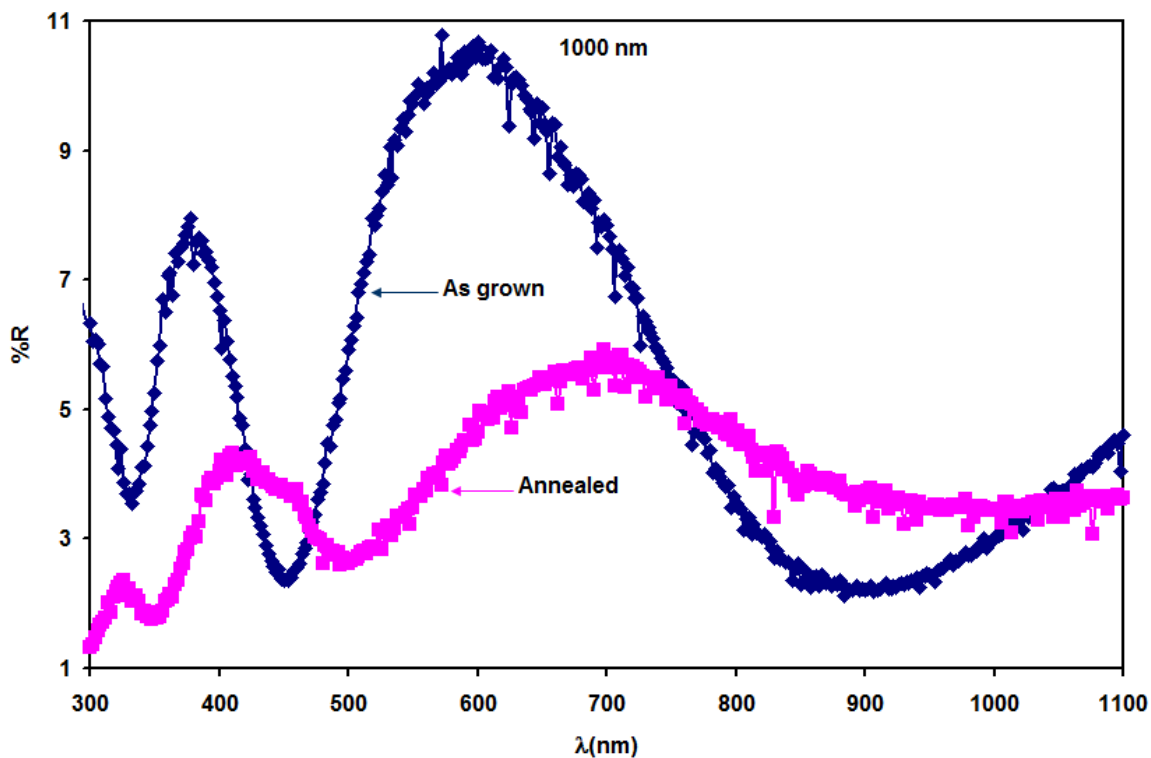


Figure 4.13: Reflection spectra of the 1000 nm CuO thin film annealed at 250 °C

Fig. 4.14 shows the variation of absorption coefficient with the photon energy for CuO at 1000 nm thickness for sample annealed at 250°C . It can be noticed that below 3.4 eV, the absorption coefficient of annealed sample, shift up on as grown sample.

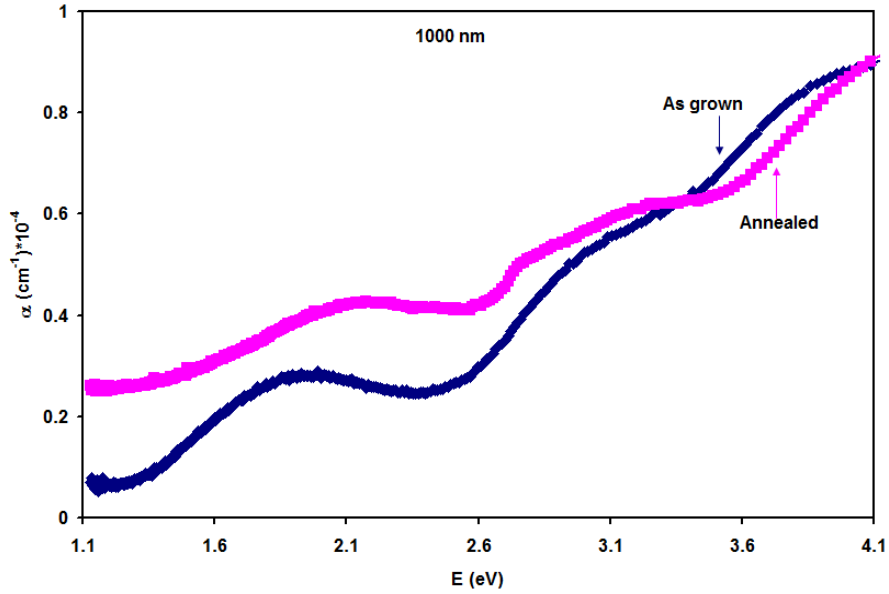


Figure 4.14 : Absorption coefficient spectra of the 1000 nm CuO thin film annealed at 250°C .

To determine the value of the energy band gap after annealing . The Tauc equation was employed again. The fitting of Tauc equation which is illustrated in Fig.4.15 reveal the band gap values which are listed in table 4.4

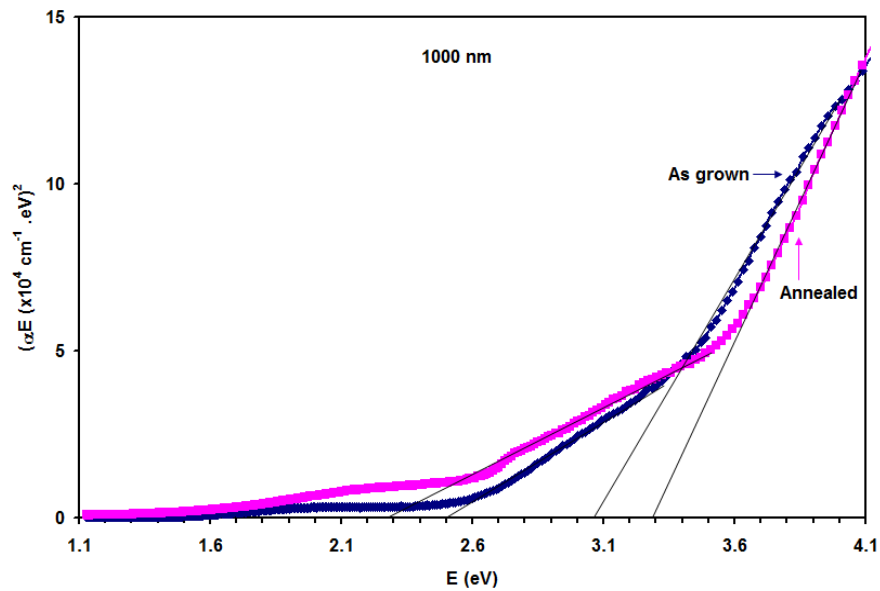


Figure 4.15: Energy band gaps investigation for the 1000 nm CuO thin films

While the band gap in the high energy region increases upon annealing, the optical gap in the visible light region decreases. It is observed that band gap value decreases after annealing. In addition, the calculated band tail width from the $\ln(\alpha) - E$ variations which is shown in Fig.4.16 revealed no band tails in the band gap of the annealed polycrystalline samples, and a band tail of width of 0.33 eV in the as grown samples. Studies on ZnO films [71] have shown that the increase in the absorption coefficient values is mostly due to the formation of band tails that allow interband transitions and hence increases the absorption coefficient values.

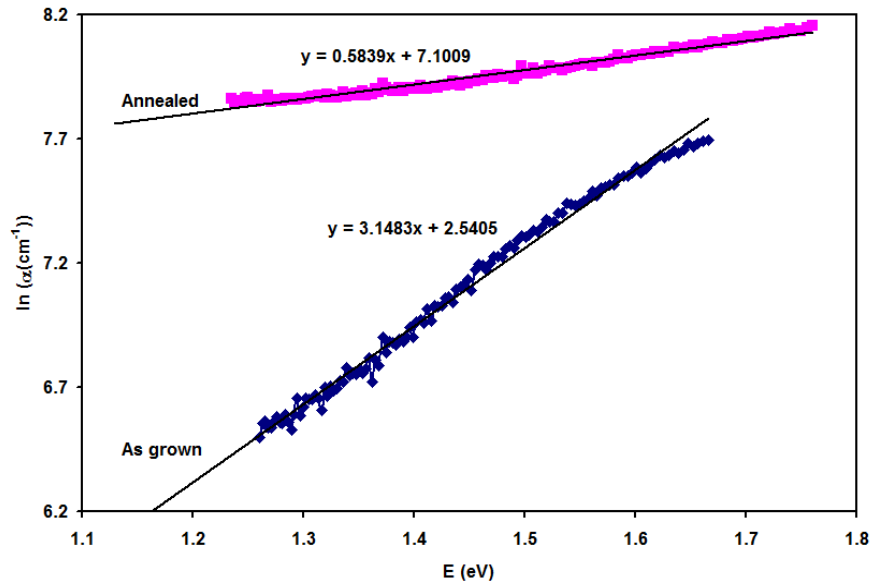


Figure 4.16: $\ln(\alpha) - E$ variation in the low absorption region for band tail investigation of the annealed 1000 nm CuO thin films at 250°C

Table 4.4: The band gaps and band tails of the 1000 nm CuO film upon annealing

d(nm)	Eg1	Eg2	Ee
1000 nm As grown	3.07	2.50	0.33
1000 nm Anealed	3.30	2.30	-----

4.5.3 Dielectric Properties

Fig.4.17 shows the effect of annealing on the dielectric constant of CuO. Significant decreases in the value of ϵ_r are observed upon annealing. The decreasing values are associated with red shift in the resonance peaks of the dielectric spectra. Particularly, the peak which was observed at 500, 793 and 1020 Hz red shifts to 430, 730 and 920 Hz respectively. The decrease in the values of the dielectric constant upon annealing can be assigned to the decrease in the degree of polarization (increasing crystallinity) [71]. The change in the lattice parameters upon annealing and the formation of regular grains indicate the reduction of the ionic displacement which in turn lower the net polarization [71].

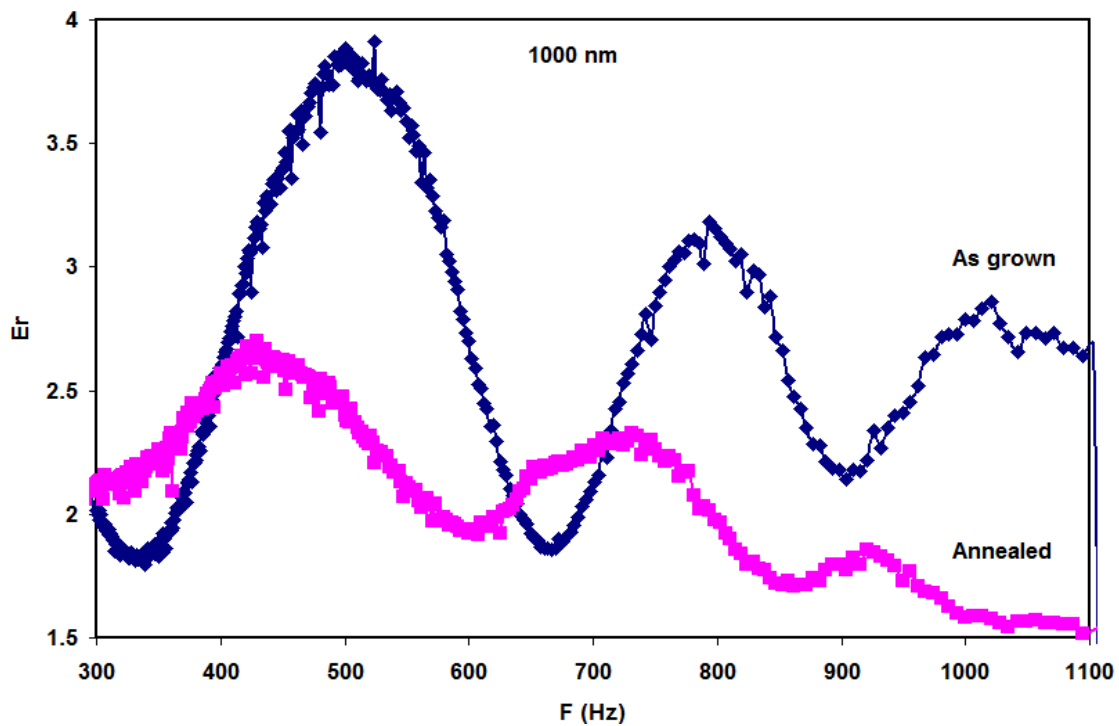


Figure 4.17: Real parts of the dielectric constant of the 1000 nm film measured in the frequency range of 300-1100 THz at 250°C annealed.

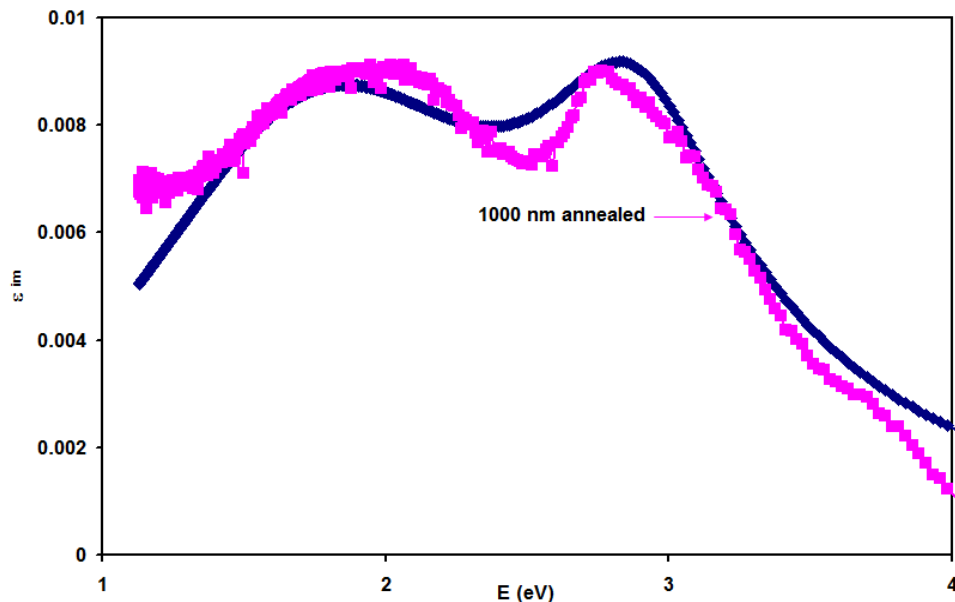


Figure 4.18: Imaginary dielectric constant of the 1000 nm CuO film measured in the frequency range of 300-1000 THz at 250°C annealed.

Table 4.5 show the effect of heat treatment on the optical conductivity parameters of CuO thin films. As the table illustrates the annealing at 250°C in vacuum media decreased the collision time by more than two times and increased the free carrier density and Plasmon frequency. This behavior is assigned to the crystalline nature of the films, which is achieved by the annealing process. Our X-ray diffraction analysis has shows that the CuO thin films convert from amorphous to polycrystalline when annealed at 250°C. The well oriented grains cause more uniform barriers and as a result holes find its way with less collision and less resistive motion as illustrated in table 4.5.

Table 4.5: The computed parameters of the Plasmon-electron interactions in the 1000 nm CuO thin films

d(nm)	1000 As grown				1000 After annealing			
i	1	2	3	4	1	2	3	4
τ_i (fs)	0.90	0.50	0.50	0.27	0.40	0.40	0.80	0.30
$W_{\epsilon i} (\times 10^{15} Hz)$	3.05	5.10	5.40	6.30	2.80	3.10	4.40	5.00
$n (\times 10^{17} cm^{-3})$	0.35	0.40	1.00	1.00	0.60	0.60	0.60	0.60
$\mu (cm^2/vs)$	17.80	9.90	9.90	5.30	7.90	7.90	15.80	5.93
$\sigma_{DC} = (n \times \mu)q$	0.099	6.34	15.84	8.48	0.076	7.58	15.17	5.69
$W_{pei} (GHz)$	0.37	0.40	0.63	0.63	0.49	0.49	0.49	0.49

In the table 4.5, the symbol (i) indicates the number of oscillation, for (i=1) the main oscillator is leader, and it the most important oscillator.

Chapter Five Conclusion

In this thesis we have developed a procedure to control the optical properties of CuO thin films. The copper oxide films which are prepared by the thermal vapor deposition technique of various thicknesses in the range of 50-1000 nm. The structural investigations the as grown films using the X-ray diffraction patterns has shown that the films are highly disordered regardless of the film thickness. Improvement of the film structure was achieved by annealing the samples for one hour in vacuum media. The annealing caused polycrystalline nature with grain sizes that increase with increasing thickness due to the increased surface morphology. Optically, thin samples whose thicknesses are less than 250 nm exhibit indirect allowed transition type of band gap. When the CuO thickness reaches 250 nm, the electronic transitions become of direct type. The annealing decreased the energy band gap in the visible light region. On the other hand, the dielectric spectral analysis has shown that the dielectric constant decreased with increasing thickness and dynamics upon annealing due to the attenuations in the polarizability. The Drude-lorentz modeling of the imaginary part of the dielectric constant has shown that the optical properties are highly influenced by the band gap type, and sample thickness owing to the large disorder degree, the free hole density decreased with increasing thickness but increased upon annealing. We conclude that the CuO thin films need to be subjected to further study to improve the crystallinity and achieve the standards prior to technological applications.

References

- [1] Kinoshita K. and Yamada T. (1992). "A new copper oxide superconductor containing carbon". *Nature*, 357:313.
- [2] M.D "preparation and Optical properties study of CuO thin film as Applied Solar Cell on LAPAN-IPB satellite " Volume 33, 2016, pages 661-667.
- [3] Ghosh, S., D. K. Avasthi, P. Shah, V. Ganesan, A.Gupta, D. Sarangi, R. Bhattacharya, W. Assmann," *Reactive magnetron sputtering of Cu₂O: Dependence on oxygen pressure and interface formation with indium tin oxide*". *Journal of Applied Physics* 109, 113704 (2011)*Vacuum* 57: 377.
- [4] I. Bobowska , P. Wojciechowski "Synthesis of nanostructures of copper compounds and their hybridisation with titanatenanosheets" *Journal of Crystal Growth* ,no.312 685–691(2010).
- [5] P A Korzhavyi, B Johansson" *Literature review on the properties of cuprous oxide Cu₂O and the process of copper oxidation*" Technical Report TR-11-08(2011).
- [6] B. K. Meyer, A. Polity, D. Reppin, M. Becker, P. Hering, P. J. Klar, Th. Sander, C. Reindl, J. Benz, M. Eickhoff, C. Heiliger, M. Heinemann, J. Bläsing, A. Krost, S. Shokovets, C. Müller, and C. Ronning "Binary copper oxide semiconductors: From materials towards devices" *Phys. Status Solidi B* 249, No. 8, 1487–1509 (2012).
- [7] Irwin, M. D. Buchholz, D. B. Hains, A. W.Chang, R. P. H.Marks, T. J." *p-Type semiconducting nickel oxide as an efficiency-enhancing anode interfacial layer in polymer bulk-heterojunction solar cells*" February 26, 2008. 105 (8) 2783-2787.
- [8] Ristov, M., Sinadinovski G. I., and I. Grozdanov, I., "Chemical deposition of Cu₂O thin films", *Thin solid films*, (1985). 123:63-67.
- [9] Riyam A. Hammoodi¹ , Assist. Prof.Dr.Ahmed K. Abbas¹ and Prof. Dr.Abdulhussein K.Eltayef. "Structural and optical properties of CuO thin films prepared via R.F.magnetron sputtering *International*" *Journal of Application or Innovation in Engineering & Management (IJAEM)* Volume 3, Issue 7, July 2014
- [10] Maria Manuel Fernandes Barbosa, "Cold Spray Deposition of Titanium onto Aluminium Substrates" Msc. Thesis ,university of Porto , Portugal.
- [11] H. Singh et alii, *Frattura ed Integrità Strutturale*, "Cold spray technology: future of coating deposition processes " 22 (2012) 69-84 .
- [12] R. Ghelichi , S. Bagherifard , M. Guagliano , M. Verani "Numerical simulation of cold spray coating" *Surface& Coatings Technology*, No. 205, 5294–5301(2011).
- [13] Pallewatta, P. G. A. P., & Grivel, J-C. "Development and application of a green-chemistry solution deposition technique for buffer layer coating on cube-textured metal

substrates in view of further deposition of rare-earth based superconductors. Department of Energy Conversion and Storage, Technical University of Denmark". (2014).page 19

[14] Armelao Lidia, DavideBarreca, Manuel Bertapelle, Gregorio Bottaro and CinziaSada and Eugenio Tondello, "*Sol-gel synthesis and characterization of CuO-based nanosystems,Materials Research Society Symposium Proceedings*". (Materials Research Society) (2003). 737: 27.

[15] Phuriwat Jittiarporn, Simona Badilescu, Mohammed N.Al Sawafta ,LekSikong ,Vo-VanTruong. "*Electrochromic properties of sol–gel prepared hybrid transition metal oxides*" Vol. 2, September 2017, Pages 286-300.

[16] Catana Andrei, Jean-Pierre Locquet, Sun M. Paik and Ivan K. Schuller, "*Local epitaxial growth of CuO films on MgO*", (1992). Phys. Rev. B46, 15477.

[17] Uma Nerle and M. K. Rabinal "*Thermal Oxidation of Copper for Favorable Formation of Cupric Oxide (CuO) Semiconductor*" ,IOSR Journal of Applied Physics, Vol. 5, (Nov. - Dec. 2013), PP 01-07.

[18]A.S.M. SayemRahmanM.A.IslamK.M.Shorowordi "*Electrodeposition and Characterization of Copper Oxide Thin Films for Solar cell Applications*" Procedia Engineering ,Vol. 105,(2015), Pages 679-685.

[19] Bruno Miguel Morais Faustino, Diogo Gomes, Jaime Faria, "*CuI p-type thin films for highly transparent thermoelectric p-n modules*" *Scientific Reports*volume 8, Article number: 6867 (2018).

[20] R. T. Downs, M. Hall-Wallace, The American Mineralogist Crystal Structure Database. American Mineralogist. 88, 247-250 (2003)

[21] K.Hyam Yoon, choi,W.Jin, and Kang, D.Heon,"*photoelectrochemical properties of copper oxide thin films coated on an n-si substrate*" Thin solid Films,Vol.372, pp.250-256, (2000).

[22]N. Serin et al, "*Annealing effects on the properties of copper oxide thin films prepared by chemical deposition*". Semicond. Sci. Technol. 20, 398 (2005)

[23] E. Tan, et al," *Crystallinity and surface effects on Young's modulus of CuO nanowires*", Applied Physics Letters, 90 pg. 163112(2007)

[24] David Adlir, "*Amorphous semiconductors*"CRC Critical reviews in solid state science, vol. 2, 1971, p: 317-465.

[25] Richard Zallen,Ronald Walter Douglas,Gerald D. Mahan "*amorphous material, amorphous substance, noncrystalline material, noncrystalline solid*"

[26] Kittel, C. (1976). *Introduction to Solid State Physics*, New York: John Wiley & Sons.ISBN 0-471-49024-5

- [27] Sitroin , Y. and M. Shaskolskaya, "*Fundamental of crystal physics*", Mir publishers, Moscow", (1982)
- [28] Tilley, Richard JD. "*Colour and the optical properties of materials: an exploration of the relationship between light, the optical properties of materials and colour*". John Wiley & Sons, 2010.
- [29] Nada M. Saeed, Journal of Al-Nahrain University, 2011, (2), pp.86-92
- [30] Jalali, Reza, et al. "*The effect of Al content, substrate temperature and nitrogen flow rate on optical band gap and optical features of nanostructured TiAlN thin films prepared by reactive magnetron sputtering.*" *Applied Physics A* 122.11 (2016): 978.
- [31] Mahdi Hasan Suhail, and Raof Ali Ahmed "*Structural, optical and electrical properties of doped copper ZnS thin films prepared by chemical spray pyrolysis technique*" *Advances in Applied Science Research*, 2014, 5(5):139-147.
- [32] Pankove, Jacques I. "*Optical processes in semiconductors*". Courier Corporation, 1971.
- [33] Fox, Mark. "*Optical properties of solids*". Vol. 3. Oxford university press, 2010.
- [34] Thakurdesai, M. , N. Kukarni , B. Chalke and A. Mahadkar, *Calcogenide Letters*.2011, 8(3),pp.223-229.
- [35] David J. Hagan and Pieter G. Kik "*OSE5312 – Light-Matter Interaction*"
- [36] S.R.Alharbi .A.F.Qasrawi "*Dielectric Dispersion in Ga2S3 Thin Films*" 8 August 2016
- [37] Fabio Caruso, Carla Verdi, Samuel Ponc'e, and Feliciano Giustino "*Electron-plasmon and electron-phonon satellites in the angle-resolved photoelectron spectra of n-doped anatase TiO2*" April 12, 2018.
- [38] Wei Cai, Ori Reinhardt, Ido Kaminer, and F. Javier Garc'ia de Abajo "*Efficient orbital angular momentum transfer between plasmons and free electrons*" May 31, 2018.
- [39] E. Ozbay, "*Plasmonics: merging photonics and electronics at nanoscale dimensions,*" *Science* 311, 189–193 (2006).
- [40] D. K. Gramotnev and S. I. Bozhevolnyi, "*Plasmonics beyond the diffraction limit,*" *Nat. Photonics* 4, 83–91 (2010).
- [41] YONGSOP HWANG, TIMOTHY J. DAVIS, JIAO LIN, AND XIAO-CONG YUAN "*Plasmonic circuit for second-order spatial differentiation at the subwavelength scale*" Vol. 26, No. 6 | 19 Mar 2018.
- [42] Askeland, Donald R., and Wendelin J. Wright ."*Science and engineering of materials*". Nelson Education, 2015.

[43] Klein, Andreas.” *Origins of limited electrical performance of polycrystalline Cu₂O thin film transistors*” .Diss. Faculdade de Cienciase Tecnologia, Unversidade NOVA de Lisboa, 2017.

[44] Min-Han Lin, perumalswamy Sekar Parasuraman and Ching-Hwa Ho .”*The study of Near-Band-Edge Property in Oxygen-Incorporated ZnS for Acting as an Efficient Crystal Photocatalyst*” June, 13,2018, pp 6351-6359 .

[45] K. S. Wong, Siarhei Zhuk, Saeid Masudy-Panah, and Goutam K. Dalapati “*Current Status and Future Prospects of Copper Oxide Heterojunction Solar Cells*” (2016)

[46] Arindam Mallick, Durga Basak, “*Revisiting the electrical and optical transmission properties of co-doped ZnO thin films as n-type TCOs*” Department of Solid State Physics, vol.96, July 2018, Pages 86-110.

[47] Julio A.N.T. Soares “*Introduction to Optical Characterization of Materials*” 2014.

[48] Aousgi,F.,and M.Kanzari.”*structural and optical properties of amorphous Sb₂S₃ thin film deposited by vacuum thermal evaporation method.*” Current Applied Physics 13.1 (2013):262-266.

[49] Qasrawi, A. F. “*Refractive index, band gap and oscillator parameters of amorphous GaSe thin films.*” Crystal research and Technology 40.6 (2005):610-614.

[50] Kim, Min-Su,et al. “*effects of Al concentration on structural and optical properties of Al-doped ZnO thin films.*”*Bulletin of the Korean Chemical Society* 33.4(2012): 1235-1241.

[51] Y. Wang, S. Lany, J. Ghanbaja, Y. Fagot-Revurat, Y. P. Chen, F. Soldera, D. Horwat, F. Mucklich, “and J. F. Pierson” *Electronic structures of Cu₂O, Cu₄O₃, and CuO: A joint experimental and theoretical study*” (2016).

[52] Habubi,N . F ., S. S. Chiad, and W. A. Jabbar. “*Effects of annealing on the Electronic Transitions of ZnS Thin Films.*” *Jornal of the ArkansasAcademy of Science* 65(2011):39.

[53] S. Agilana , D. Mangalarajb,, Sa.K. Narayandassb , G. Mohan Raoc “ *Effect of thickness and substrate temperature on structure and optical band gap of hot wall-deposited CuInSe₂ polycrystalline thin films* ” 3 May 2005 page 98 .

[54] F. Yakuphanoglu , M. Sekerci , A. Balaban “ *The effect of film thickness on the optical absorption edge and optical constants of the Cr(III) organic thin films* ”*Optical Materials* 27 (2005) page 1370-1371.

[55] S.R. Ovshinsky, D. Adler, *Contemp. Phys.* 19 (1978) 109.

[56] Su-Shia Lin, Jow-Lay Huang “*Effect of thickness on the structural and optical properties of ZnO films by r.f. magnetron sputtering*” *Surface & Coatings Technology* 185 (2004) page 224 .

- [57] Su-Shia Lin, Jow-Lay Huang “*Effect of thickness on the structural and optical properties of ZnO films by r.f. magnetron sputtering*” May 2004, p.224-227 .
- [58] Y.Wang, P.Miska, D.Pilloud, D.Horwat, F.Mucklich, and J. F. Pierson. “*Transmittance enhancement and optical band gap widening of Cu₂O thin films after air annealing*” J appl phy 115 , 073505 (2014)
- [59] Yongqian Wang Tingting Jiang Dawei Meng JunYang Yinchang LiQun MaJunHan “*Fabrication of nanostructured CuO films by electrodeposition and their photocatalytic properties*” Vol.317, 30 October 2014, Pages 414-421.
- [60] Xing-Qiu Chen, C. L. Fu, C. Franchini, and R. Podloucky “*Hybrid density-functional calculation of the electronic and magnetic structures of tetragonal CuO*” (2009) .
- [61] “*Drude-Lorentz Model for Dispersion in Dielectrics*” J.ph4 . D ; Appl . phs(244011) 155405 .
- [62] Hryciw, Aaron, Young Chul Jun, and Mark L. Brongersma.” *Plasmonics: Electrifying plasmonics on silico* “Nature materials 9.1(2010): 3-4.
- [63] Eldlio, Mohamed, Franklin Che, and Micheal Cada. “*Drude-Lorentz Model of Semiconductor Optical Plasmons*. “IAENG Transactions on Engineering Technologies springer Netherlands, 2014.41-49
- [64] M Abaker, Ahmad Umar, S Baskoutas, S H Kim and S W Hwang, “*Structural and optical properties of CuO layered hexagonal discs synthesized by a low-temperature hydrothermal process*” (March 2011).
- [65] Kumar, Rajesh, Paramjit Singh, S. K. Gupta, R. Gupta, M. K. Jaiswal, M. Prasad, A. Roychowdhury, R. P. Chauhan, and D. Das. "Radiation induced nano-scale free volume modifications in amorphous polymeric material: a study using positron annihilation lifetime spectroscopy." Journal of Radioanalytical and Nuclear Chemistry 314, no. 3 (2017): 1659-1666.
- [66] Suresh, R., V. Ponnuswamy, C. Sankar, M. Manickam, and R. Mariappan. "Influence of Co concentration on the structural, optical, morphological and photo-diode properties of cerium oxide thin films." Ceramics International 42, no. 11 (2016): 12715-12725.
- [67] Osamah A. Bin-Dahman,^{1,2} Mostafizur Rahaman,³ Dipak Khastgir⁴ and Mamdouh A. Al-Harhi “*Electrical and Dielectric Properties of Poly(Vinyl Alcohol)/Starch/Graphene Nanocomposites*” (2017) Vol. 9999
- [68] Cheng, Shao-Liang, and Ming-Feng Chen. "Fabrication, characterization, and kinetic study of vertical single-crystalline CuO nanowires on Si substrates." Nanoscale research letters⁷, no. 1 (2012): 119.

[69] "Effect of Thickness on the Structure and Properties of ZnO Thin Films Prepared by Pulsed Laser Deposition" Japanese Journal of Applied Physics Vol. 45, No. 10A, 2006, pp. 7860–7865 .

[70] Martin, F., P. Muralt, M-A. Dubois, and A. Pezous. "Thickness dependence of the properties of highly c-axis textured AlN thin films." Journal of Vacuum Science & Technology A: Vacuum, Surfaces, and Films 22, no. 2 (2004): 361-365.

[71] Xue, S. W., X. T. Zu, W. L. Zhou, H. X. Deng, X. Xiang, L. Zhang, and H. Deng. "Effects of post-thermal annealing on the optical constants of ZnO thin film." Journal of Alloys and Compounds 448, no. 1-2 (2008): 21-26

Table of symbols

Shortcut	Meaning
A	Absorbance
AFM	Atomic force microscopy
Ar	Argon
α	Absorption coefficient
CS	Cold spray
CSD	Chemical solution deposition
CVD	Chemical vapor deposition
D	Grain size
ϵ_{im}	Imaginary component of dielectric
ϵ_r	Real component of dielectric
EDS	Energy dispersive spectroscopy
eV	Electron volt
FTO	Fluorine doped Tin Oxide
I	Intensity
λ	Wave length

LSP	Localized surface Plasmon
μ	Drift mobility
M	Molecular concentration
m^*	Effective mass
N	Free charge carrier density
Ni	Nickel
NIR	Near infra red
Nm	Nanometer
NPs	Novel metal oxide
PVD	Physical vapor deposition
R	Reflectance
R.F.	Radio frequency
SEM	Scanning electron microscope
SOFCs	Solid oxide fuel cells
τ	Free carrier scattering time
T	Transmittance
UV	Ultraviolet
VIS	Visible light region

ω_e	Resonant frequency
ω_{pe}	Electron bounded plasma frequency
XRD	X-ray diffraction

، يظهر الطيف الثابت العازل الذي ينفذ في نطاق الطاقة من 1.1-4.0 eV قيمًا متناقصة مع زيادة سماكة العينة. تم تصميم الجزء التخليبي من الأطياف العازلة طبقاً لتفاعل الثغرة في الكشف عن معلمات التوصيل البصرية. وقد أظهرت المعلمات التي تم تقييمها أنه يمكن استخدام أفلام CuO الرقيقة كمرنانات بصرية مع نسبية التوصيلية البصرية المناسبة المناسبة لاتصالات الضوء المرئي.

تأثير السماكة و ما بعد التلدين على الخواص الهيكلية و البصرية و العازلة للأغشية الرقيقة لأكسيد النحاس

الملخص

في هذا العمل ، يتم استكشاف سماكة الغشاء الرقيق وتأثيرات ما بعد التلدين على الخواص التركيبية والتركيبية والبصرية للأغشية الرقيقة لأكسيد النحاس عن طريق حيود الأشعة السينية والتحليل الطيفي للأشعة السينية المشتتة للطاقة وتقنيات طيف الضوء المرئي فوق البنفسجي المرئي ، على التوالي. بشكل خاص ، تم إنتاج العديد من الأغشية الرقيقة لأكسيد النحاس ، والتي تظهر السماكة في نطاق 50-1000 نانومتر بواسطة تقنية ترسيب البخار الفيزيائي تحت ضغط مفرغ من 10-5 مبار. إن التأثيرات السميكة للأغشية على الطبيعة البلورية وعلى النفاذية البصرية ، الانعكاسية ، الامتصاصية وكذلك الفجوة في نطاق الطاقة والأطياف العازلة مصممة على تحديد السماكة الأكثر ملاءمة للتطبيقات الإلكترونية البصرية. ولوحظ أنه في حين أن الأفلام التي يتراوح سمكها بين 50 و 100 نانومتر تسمح بشكل غير مباشر بفارق نطاق الانتقال الإلكتروني ، فإن أفلام السماكة الأكبر تظهر فجوة نطاق الطاقة الانتقالية المباشرة. بالإضافة إلى ذلك ، فقد أظهر تحليل أطياف معامل الامتصاص في منطقة الامتصاص المنخفض أنه باستثناء الأفلام التي يبلغ سمكها 1000 نانومتر ، فإن جميع أفلام CuO تعرض ذيل نطاق عرض نطاق الطاقة في نطاق 0.29 - 0.66 فولت. تم أيضًا تلميع طبقة رقيقة 1000 نانومتر في الفراغ عند درجة حرارة 250 درجة مئوية ، وتمت دراسة تأثير درجة حرارة التلدين على الخصائص البنيوية والضوئية والديالكترية باستخدام تقنيات التوصيف المختلفة. أكد تحليل XRD على التبلور المعزز لعينة سمك 1000 نانومتر. تم قياس فجوات النطاق البصري للفيلم الرفيع المجهد 1000 نانومتر CuO إلى 3.30 و 3.20 eV ، وعرض الفيلم الرفيع 1000 نانومتر ذيل عصابة بعد أن يساوي الصلب 0.58 eV. من ناحية أخرى

